Atmospheric
Chemistry
and Physics

Open Access

Comparison of the HadGEM2 climate-chemistry model against in situ and SCIAMACHY atmospheric methane data

G. D. Hayman[1], F. M. O'Connor[2], M. Dalvi[2], D. B. Clark[1], N. Gedney[3], C. Huntingford[1], C. Prigent[4], M. Buchwitz[5], O. Schneising[5], J. P. Burrows[5], C. Wilson[6], N. Richards[6], and M. Chipperfield[6]

[1]Centre for Ecology and Hydrology, Crowmarsh Gifford, Wallingford, OX10 8BB, UK
[2]Met Office Hadley Centre, FitzRoy Road, Exeter, EX1 3PB, UK
[3]Joint Centre for Hydrometeorological Research, Met Office Hadley Centre,
Crowmarsh Gifford, Wallingford, OX10 8BB, UK
[4]CNRS-LERMA, Observatoire de Paris, 61 avenue de l'Observatoire, 75014 Paris, France
[5]Institute of Environmental Physics, University of Bremen FB1, P. O. Box 330440,
Otto Hahn Allee 1, 28334 Bremen, Germany
[6]School of Earth and Environment, University of Leeds, Leeds, LS2 9JT, UK

Correspondence to: G. D. Hayman (garr@ceh.ac.uk)

Abstract. Wetlands are a major emission source of methane (CH_4) globally. In this study, we evaluate wetland emission estimates derived using the UK community land surface model (JULES, the Joint UK Land Earth Simulator) against atmospheric observations of methane, including, for the first time, total methane columns derived from the SCIAMACHY instrument on board the ENVISAT satellite.

Two JULES wetland emission estimates are investigated: (a) from an offline run driven with Climatic Research Unit–National Centers for Environmental Prediction (CRU-NCEP) meteorological data and (b) from the same offline run in which the modelled wetland fractions are replaced with those derived from the Global Inundation Extent from Multi-Satellites (GIEMS) remote sensing product. The mean annual emission assumed for each inventory (181 Tg CH_4 per annum over the period 1999–2007) is in line with other recently published estimates. There are regional differences as the unconstrained JULES inventory gives significantly higher emissions in the Amazon (by ~ 36 Tg CH_4 yr^{-1}) and lower emissions in other regions (by up to 10 Tg CH_4 yr^{-1}) compared to the JULES estimates constrained with the GIEMS product.

Using the UK Hadley Centre's Earth System model with atmospheric chemistry (HadGEM2), we evaluate these JULES wetland emissions against atmospheric observations of methane. We obtain improved agreement with the surface concentration measurements, especially at high northern latitudes, compared to previous HadGEM2 runs using the wetland emission data set of Fung et al. (1991). Although the modelled monthly atmospheric methane columns reproduce the large-scale patterns in the SCIAMACHY observations, they are biased low by 50 part per billion by volume (ppb). Replacing the HadGEM2 modelled concentrations above 300 hPa with HALOE–ACE assimilated TOMCAT output results in a significantly better agreement with the SCIAMACHY observations. The use of the GIEMS product to constrain the JULES-derived wetland fraction improves the representation of the wetland emissions in JULES and gives a good description of the seasonality observed at surface sites influenced by wetlands, especially at high latitudes. We find that the annual cycles observed in the SCIAMACHY measurements and at many of the surface sites influenced by non-wetland sources cannot be reproduced in these HadGEM2 runs. This suggests that the emissions over certain regions (e.g. India and China) are possibly too high and/or the monthly emission patterns for specific sectors are incorrect.

The comparisons presented in this paper show that the performance of the JULES wetland scheme is comparable to that of other process-based land surface models. We identify

areas for improvement in this and the atmospheric chemistry components of the HadGEM Earth System model. The Earth Observation data sets used here will be of continued value in future evaluations of JULES and the HadGEM family of models.

1 Introduction

The global mean atmospheric concentration of methane (CH_4) has increased from ~ 700 parts per billion by volume (ppb) at the start of the industrial era to ~ 1808 ppb in 2012 (Blunden and Arndt, 2013) and constitutes $\sim 20\%$ of the anthropogenic radiative forcing by greenhouse gases (Forster et al., 2007). Increases in atmospheric CH_4 concentrations potentially have a large impact on the global climate, through its direct radiative forcing effect (the radiative efficiency of CH_4 is about 10 times greater than that of carbon dioxide per tonne emitted: Ramaswamy et al., 2001) and, indirectly, through the formation of tropospheric ozone and aerosols (Shindell et al., 2009). In consequence, control of CH_4 emissions is potentially an important lever for international climate change policy and possible (short-term) mitigation actions (e.g. Shindell et al., 2012; Bowerman et al., 2013). An accurate knowledge of its contemporary sources and sinks is therefore essential.

CH_4 is emitted to the atmosphere from a number of sources (Denman et al., 2007): (a) biogenic sources, covering wetlands, agriculture (livestock and rice production), landfills, forests, oceans and termites, and (b) non-biogenic sources, comprising fossil-fuel mining and burning, biomass burning, waste treatment and geological sources. The major removal process for CH_4 in the atmosphere is reaction with hydroxyl (OH) radicals. Minor sinks are reactions with chlorine (Cl) atoms in the boundary layer, reactions with OH, Cl and excited oxygen atoms ($O(^1D)$) in the stratosphere, and uptake by soils. The overall atmospheric lifetime of CH_4 is estimated to be 9.1 ± 1.9 years (Prather et al., 2012).

In situ measurements of CH_4 concentrations have been made from global networks of surface atmospheric sites since the 1980s (Steele et al., 1987, 1992; Blake and Rowland, 1988; Dlugokencky et al., 1994b, 1998, 2001, 2003, 2009, 2011; Rigby et al., 2008). The globally averaged CH_4 growth rate, derived from the surface measurements, has fallen from a high of 16 ppb yr^{-1} in the late 1970s/early 1980s (Blake and Rowland, 1988; Steele et al., 1992; Dlugokencky et al., 1998) to almost zero between 1999 and 2006 (Dlugokencky et al., 2011). This period of declining or low growth was however interspersed with years of positive growth-rate anomalies (e.g. in 1991–1992, 1998–1999 and 2002–2003). Since 2007, renewed growth has been evident (Rigby et al., 2008; Dlugokencky et al., 2009), with the largest increases observed to originate over polar northern latitudes and the Southern Hemisphere (SH) in 2007 and

in the tropics in 2008. There is significant concern that this might be the restart of an ongoing upward trend in atmospheric CH_4 concentrations.

The observed interannual variability in atmospheric CH_4 concentrations and the associated changes in growth rates have variously been ascribed to changes in the different CH_4 sources and sinks: (a) CH_4 sources directly influenced by human activities, such as fossil fuel production (Dlugokencky et al., 1994b, 2011; Bousquet et al., 2006; Bergamaschi et al., 2013; Kirschke et al., 2013), (b) wetland emissions (Bousquet et al., 2006, 2011; Ringeval et al., 2010; Kirschke et al., 2013; Pison et al., 2013) and (c) biomass burning, especially during the intense El Niño years in 1997 and 1998 (Dlugokencky et al., 2001; Kirschke et al., 2013). The most likely causes of the CH_4 anomalies observed during 2007 and 2008 were the anomalously high temperatures in the Arctic (Dlugokencky et al., 2009) or larger CH_4 emissions from natural wetlands in tropical South America and boreal Eurasia (Bousquet et al., 2011).

Atmospheric column CH_4 measurements with sensitivity to the surface and lower troposphere are now available from satellite instruments: SCIAMACHY on ENVISAT from 2003 (Buchwitz et al., 2005; Frankenberg et al., 2005; Schneising et al., 2009, 2011) and, since 2009, the Greenhouse Gas Observing Satellite (GOSAT, Kuze et al., 2009). The satellite measurements complement the observations from the sparse network of surface sites. Frankenberg et al. (2006) concluded that the SCIAMACHY measurements could be used in inverse modelling and were an important step in reducing the uncertainties in the global methane budget. Bergamaschi et al. (2007) extended the inverse modelling analysis to include both surface and satellite observations. Their results indicated significantly greater CH_4 emissions in the tropics compared to either the a priori estimates or the inversion based on the surface measurements alone. The discrepancy was partially reduced after taking account of spectroscopic changes to interfering water vapour absorption lines (Frankenberg et al., 2008; Meirink et al., 2008). More recently, Fraser et al. (2013) have used column CH_4 measurements from the Thermal and Near-infrared Sensor for Carbon Observation (TANSO) on the GOSAT to estimate global and regional monthly CH_4 fluxes.

The surface and satellite atmospheric measurements have been used to constrain the total global annual source strength of CH_4 (in Tg CH_4 yr^{-1}): 550 ± 50 (Frankenberg et al., 2005); 582 (Denman et al., 2007); 515 ± 3 (1999–2006), 536 (2007) and 533 (2008) (Bousquet et al., 2011); 513 ± 9 (1990s) and 514 ± 14 (2000s) (TRANSCOM Methane Model Intercomparison, Patra et al., 2011), 510–516 (2009–2010) (Fraser et al., 2013) and 551(500–592) (1980s), 554(529–596) (1990s) and 548(526–569) (2000s) (Kirschke et al., 2013). However, there remain considerable uncertainties in the partitioning of sources and their spatial and temporal distribution (Kirschke et al., 2013).

Wetlands are generally accepted as being the largest, but least well quantified, single natural source of CH_4, with global emission estimates ranging from 100 to 231 $Tg\,CH_4\,yr^{-1}$ (Denman et al., 2007; USEPA, 2010). The modelling of wetlands and their associated emissions of CH_4 has become the subject of much current interest. The review by Melton et al. (2013) provides a summary of the current state of knowledge on wetlands and the outcome of the WETland and Wetland CH_4 Inter-comparison of Models project (WETCHIMP). Melton et al. (2013) found a large variation in the wetland areas and associated CH_4 emissions from the participating models and varying responses to climate change (as represented by increases in the driving CO_2 concentrations, temperature and precipitation).

Wetland emissions are particularly sensitive to climate change (O'Connor et al., 2010; Melton et al., 2013). Gedney et al. (2004) concluded that the wetlands model used in the Joint UK Land Earth Simulator (JULES, the UK community land surface model) would lead to a doubling of CH_4 emissions from wetlands by 2100 for the IPCC IS92a scenario considered. As a major emission source of CH_4 which responds strongly to climate change, it is vital that the description of wetlands and the associated emissions of CH_4 used in land surface and climate models reflects current understanding and the implications of emerging data sets.

In this paper, we use atmospheric observations of CH_4 (surface concentrations and total columns derived from the SCIAMACHY instrument) to evaluate simulations of the Hadley Centre's Global Environmental Model (HadGEM2, Collins et al., 2011) and hence to assess the wetland methane emission parameterization used in JULES. The paper is structured as follows. Sect. 2 provides a brief description of the models, the experimental set-up and the key data sets used in the model runs and subsequent analysis. Sect. 3 compares the modelled CH_4 concentrations with atmospheric methane measurements and includes discussion of the results. Finally, conclusions can be found in Sect. 4.

2 Approach and methodology

2.1 HadGEM2

2.1.1 Model configuration and nudging

HadGEM is a family of models which have been designed to simulate and understand the centennial-scale evolution of climate, including biogeochemical feedbacks, in response to anthropogenic and natural greenhouse gas and aerosol-precursor emissions. In this study, we used version 2 of HadGEM (HadGEM2: Collins et al., 2011) in an atmosphere-only configuration. The model was driven with sea-surface temperature and sea ice fields taken from the second Atmosphere Model Intercomparison Project (www-pcmdi.llnl.gov/projects/amip). The dynamics and tempera-

tures of the climate model were "nudged" (Telford et al., 2008) towards the European Centre for Medium-Range Weather Forecasts (ECMWF) ERA-40 reanalyses (Uppala et al., 2005) of the atmospheric state of temperature, surface pressure and the horizontal wind components. Hence, the synoptic variability would be similar to that observed, improving the comparison with observations of atmospheric trace constituents.

2.1.2 Atmospheric chemistry

For the runs reported here, we use the standard tropospheric chemistry scheme (O'Connor et al., 2014) from the UK Chemistry and Aerosol (UKCA; http://www.ukca.ac.uk) model, which has been implemented into HadGEM2. This chemistry scheme comprises 46 chemical species (of which 26 are advected tracers), 129 reactions (102 gas-phase and 27 photolysis reactions) and interactive deposition schemes. The chemistry scheme simulates the chemical cycles of odd oxygen (O_x), odd hydrogen (HO_x) and oxides of nitrogen (NO_x) and the oxidation of carbon monoxide (CO), CH_4, ethane (C_2H_6) and propane (C_3H_8). There are eight emitted species: CO, NO_x, CH_4, C_2H_6, C_3H_8, HCHO (formaldehyde), CH_3CHO (acetaldehyde) and CH_3COCH_3 (acetone). In relation to CH_4, although the dominant loss of CH_4 in the troposphere is through oxidation by the hydroxyl radical (OH), oxidation in the stratosphere is solely represented by reactions with OH and $O(^1D)$; there is no oxidation by Cl. However, because the upper model boundary is at 39 km, oxidation by $O(^1D)$ does not provide a sufficiently large sink for CH_4. Hence, an explicit loss term is applied at the top of the model domain to compensate for the lack of stratospheric CH_4 oxidation. Further details on the standard tropospheric chemistry scheme and its evaluation can be found in O'Connor et al. (2014).

2.1.3 Land surface module

JULES is a physically based model that describes the water, energy and carbon balances and includes temperature, moisture and carbon stores (Best et al., 2011; Clark et al., 2011). JULES can be run as a stand-alone model using appropriate driving meteorological data or as the land surface component in UK climate or earth system models (note that HadGEM2 strictly uses the Met Office Surface Exchange System, an earlier version of JULES, as the land surface component).

JULES uses a tiled approach to describe subgrid-scale heterogeneity. Nine surface types are used, of which five are vegetation-related. The fractions of surface types within each land-surface grid box can either be modelled or prescribed. Air temperature, humidity, wind speed and incident radiation above the surface and soil temperatures and moisture contents below the surface are treated as homogeneous across a grid cell; other parameters are calculated for each surface type.

The current version of JULES uses a methane wetland emission parameterization, developed and tested by Gedney et al. (2004) for use at large spatial scales. The wetland parameterization is coupled to the large-scale hydrology scheme of Gedney and Cox (2003), which predicts the distribution of subgrid-scale water table depth and wetland fraction (f_w) from the overall soil moisture content and the subgrid-scale topography. The methane flux from wetlands $F_w(CH_4$ in $kg\,C\,m^{-2}\,s^{-1})$ is given in terms of the main controls of temperature, water table and substrate availability:

$$F_w(CH_4) = f_w\, k(CH_4)\, C_s\, Q_{10}(T_{soil})^{(T_{soil}-T_0)/10}, \tag{1}$$

where T_{soil} is the soil temperature (in K) averaged over the top 10 cm and $k(CH_4)$ is a global constant which is calibrated to give the required global methane flux. Soil carbon content (C_s in $kg\,C\,m^{-2}$) was used as there is a lack of global data on substrate availability. The default parameter values are $k(CH_4) = 7.4 \times 10^{-12}\,s^{-1}$, $T_0 = 273.15$ K and $Q_{10}(T_0) = 3.7$ (Clark et al., 2011).

2.2 Earth Observation data sets

We have used a number of key Earth Observation data sets, either to constrain the land surface and chemistry–climate models or to evaluate the models. These are briefly described in the following sections.

2.2.1 Wetland and inundation dynamics

A globally applicable remote-sensing technique, employing a suite of complementary satellite observations, has been developed to derive wetland inundation extents: the Global Inundation Extent from Multi-Satellites (GIEMS) (Prigent et al., 2001b, 2007; Papa et al., 2010; Prigent et al., 2012). The method estimates inundation and its seasonal and spatial dynamics at the global scale using three sensors. Detection of inundation primarily relies on the passive microwave land-surface signal between 19 and 85 GHz from the Special Sensor Microwave/Imager (SSM/I). Relative to non-flooded lands, inundated regions are characterized by low microwave emissivities and high-emissivity polarization difference, even under dense canopies. In semi-arid regions where bare surfaces and inundation can produce similar SSM/I signatures, the Normalized Difference Vegetation Index (NDVI), derived from visible and near-infrared reflectances from the Advanced Very High Resolution Radiometer (AVHRR), is used to resolve ambiguities. Active microwave backscattering at 5.25 GHz from the ASCAT scatterometer (the original method used the scatterometer on board the European Remote Sensing (ERS) satellite) is very sensitive to vegetation density (Prigent et al., 2001a). These measurements are used to assess vegetation contributions and to quantify the fraction of inundation within the pixel. The GIEMS data set is now available on a monthly basis from 1993 to 2007 globally, and mapped on an equal area grid

of 773 km^2 (equivalent to $0.25° \times 0.25°$ at the equator) (Prigent et al., 2012). This and the earlier data sets have been thoroughly evaluated by comparison with other static estimates of wetland extent. This product is the only dynamic estimate available. It has also been compared with related hydrological variables such as rain rate, river gauges and river heights (Prigent et al., 2001b, 2007; Papa et al., 2006a, b, 2007, 2008a, b).

2.2.2 SCIAMACHY atmospheric column methane

Atmospheric column-averaged CH_4 dry-air mixing ratios (XCH_4 in ppb) are available from the SCIAMACHY instrument on the ENVISAT satellite (Schneising et al., 2009, 2011). The SCIAMACHY data product used in this study was retrieved from nadir measurements using the Weighting Function Modified Differential Optical Absorption Spectroscopy (WFM-DOAS) processing algorithm (version 2.3, WFMDv2.3). WFMDv2.3 is an improved version of WFMDv2.0.2 (Schneising et al., 2011, 2012), using a correction factor depending on simultaneously retrieved water vapour abundance (from the same fitting window as CO_2, which is used as a proxy for the light path) to account for spectroscopic interferences. The WFM-DOAS algorithm is one of the algorithms currently being compared in the European Space Agency (ESA) project: Greenhouse Gases Climate Change Initiative (GHG-CCI; Buchwitz et al., 2013). The SCIAMACHY data set has been validated and its relative accuracy, a quality measure quantifying regional biases, is 7.8 ppb (Dils et al., 2014). The SCIAMACHY XCH_4 data set was provided on a $0.5° \times 0.5°$ grid at monthly intervals for the time period 2003–2009. It was regridded to the spatial resolution of the HadGEM2 model to enable direct comparison with the model.

2.2.3 HALOE–ACE assimilated TOMCAT

The Halogen Occultation Experiment (HALOE, Russell et al., 1993) provides solar occultation observations of a range of trace gases including CH_4 (Park et al., 1996) from September 1991 until November 2005. Observations were obtained at about 15 sunrise and sunset locations per day. The Atmospheric Chemistry Experiment (ACE, Bernath et al., 2005) was launched onboard SCISAT-1 in August 2003 and since then has been providing solar occultation observations of trace gases including CH_4 (De Mazière et al., 2008). Despite the geographical sparseness of these data sets, the long atmospheric lifetime of CH_4 means that these solar occultation data are sufficient to constrain a stratospheric chemical transport model (CTM) through data assimilation (see Chipperfield et al., 2002). In this study, we use the TOMCAT offline 3-D CTM (Chipperfield, 2006; Breider et al., 2010; Monks et al., 2012), with data assimilation of the HALOE and ACE measurements, to provide monthly CH_4 concentra-

tion fields for the upper troposphere and stratosphere for the years 2000 through to 2007 (see Sect. 3.2.1).

2.3 Model runs and emission inventories

2.3.1 Wetland methane emissions

For their CH_4 wetland emissions, O'Connor et al. (2014) aggregate the wetlands, bogs, swamps and tundra components in the data set of Fung et al. (1991), available from http://data.giss.nasa.gov/ch4_fung/. This aggregated wetland emission data set (totally 181 $Tg\,CH_4\,yr^{-1}$), together with the other CH_4 emission sources used, was found to give very reasonable atmospheric CH_4 lifetimes and burdens and global mean concentrations, and reasonably good comparisons with in situ surface atmospheric observations. One of the runs undertaken in this study made use of this inventory (denoted FUNG below). We now believe our use of the data set to be incorrect. The components in the data set represent two different emission scenarios with different assumptions on seasonality (Fung et al., 1991). We also use the version of the Fung inventory produced for the TRANSCOM–CH_4 study (Patra et al., 2009, 2011), denoted TRANSCOM-FUNG below. This was rescaled to give a global annual emission flux of 181 $Tg\,CH_4\,yr^{-1}$, as this was the nominal total wetland emission used in previous work.

The other runs reported here use methane wetland emissions derived from an offline global run of the JULES land surface model (see Sect. 2.1.3), driven with CRU-NCEP meteorological data (Viovy and Ciais, 2009), for $0.5° \times 0.5°$ terrestrial grid squares (denoted JULES). A second emission estimate is derived from this offline JULES run by replacing the modelled wetland fraction in Eq. (1) with the wetland fraction derived from the regridded GIEMS product (denoted JULES-GIEMS). As the GIEMS inundation product does not discriminate between natural wetlands and managed water areas such as rice paddy fields, the GIEMS product is corrected for such rice paddy fields, using information on the area of cultivation of rice from both irrigated and rain-fed cultivation (Portmann et al., 2010). The two JULES emission estimates are separately scaled so that the average global annual emission flux over the period of the model runs (1999–2007) is 181 $Tg\,CH_4\,yr^{-1}$, for the reason given in the previous paragraph.

The most noticeable differences between the JULES emission data sets and those of Fung et al. (1991) are the significantly higher emissions in the boreal region ($> 50°$ N) in both the FUNG data set as used by O'Connor et al. (2014) and the TRANSCOM-FUNG inventory compared to the JULES-based inventories (FUNG: ~ 90; TRANSCOM-FUNG: ~ 52; JULES: ~ 5 and JULES-GIEMS: $\sim 15\,Tg\,CH_4\,yr^{-1}$), and conversely the higher emissions in the tropics ($30°$ S–$30°$ N) in the JULES-based inventories (FUNG: ~ 67; TRANSCOM-FUNG: ~ 100; JULES: ~ 167 and JULES-GIEMS: $\sim 127\,Tg\,CH_4\,yr^{-1}$).

This can be seen in Fig. 1 (see discussion in Sect. 3.3.2) and also Fig. 3 of the Supplement.

Additional information on the wetlands and their associated emissions of methane is provided in Sect. 1.1 of the Supplement.

2.3.2 Other emissions

We generate year- and month-specific emission data sets for the period from 1997 to 2009 for the emitted species in the UKCA standard tropospheric chemistry scheme (see Sect. 2.1.2). The approach adopted varies depending on the source sector:

- *Anthropogenic*: year- and month-specific emission data sets are derived from the decadal-averaged emission inventories compiled by Lamarque et al. (2010), by scaling the emission totals for the different years and source sectors using sector and species-specific scaling factors based on the annual trends given in various EDGAR time series.

- *Biomass burning*: year-specific emission inventories are available from the Global Fire Emissions Database (GFED, v3.1) for the years 1997 to 2009 (van der Werf et al., 2010), on a monthly time step. The CH_4 emissions are rescaled to give the same period mean (25 $Tg\,CH_4$ per annum) as used in the UKCA runs of O'Connor et al. (2014).

- *Other*: data on sources such as termites and hydrates for CH_4 and oceanic emissions of CH_4 and other volatile organic compounds are taken from various sources, as described in O'Connor et al. (2014). These data sets contain a single annual cycle, which is assumed to apply for all years.

A number of studies (e.g. Monteil et al., 2011; Patra et al., 2011) find that the anthropogenic trend in the 2000s as given in the EDGAR v4.2 emission time series is not consistent with surface atmospheric measurements of methane and its ^{13}C isotope for the period from 2000 to 2006. For this reason, we prefer to use the earlier EDGAR v3.2 emission time series. The recently published papers by Bergamaschi et al. (2013) and Kirschke et al. (2013) provide justification for this choice.

Additional information on the emission data sets used for the other emitted species in the model runs is provided in Sect. 1.2 of the Supplement.

3 Results and discussion

Four HadGEM2 runs were undertaken for the period 1999–2007, which differed only in the wetland emission inventory used (FUNG, TRANSCOM-FUNG, JULES and JULES-GIEMS). Figure 2 shows the spatial distribution of the global
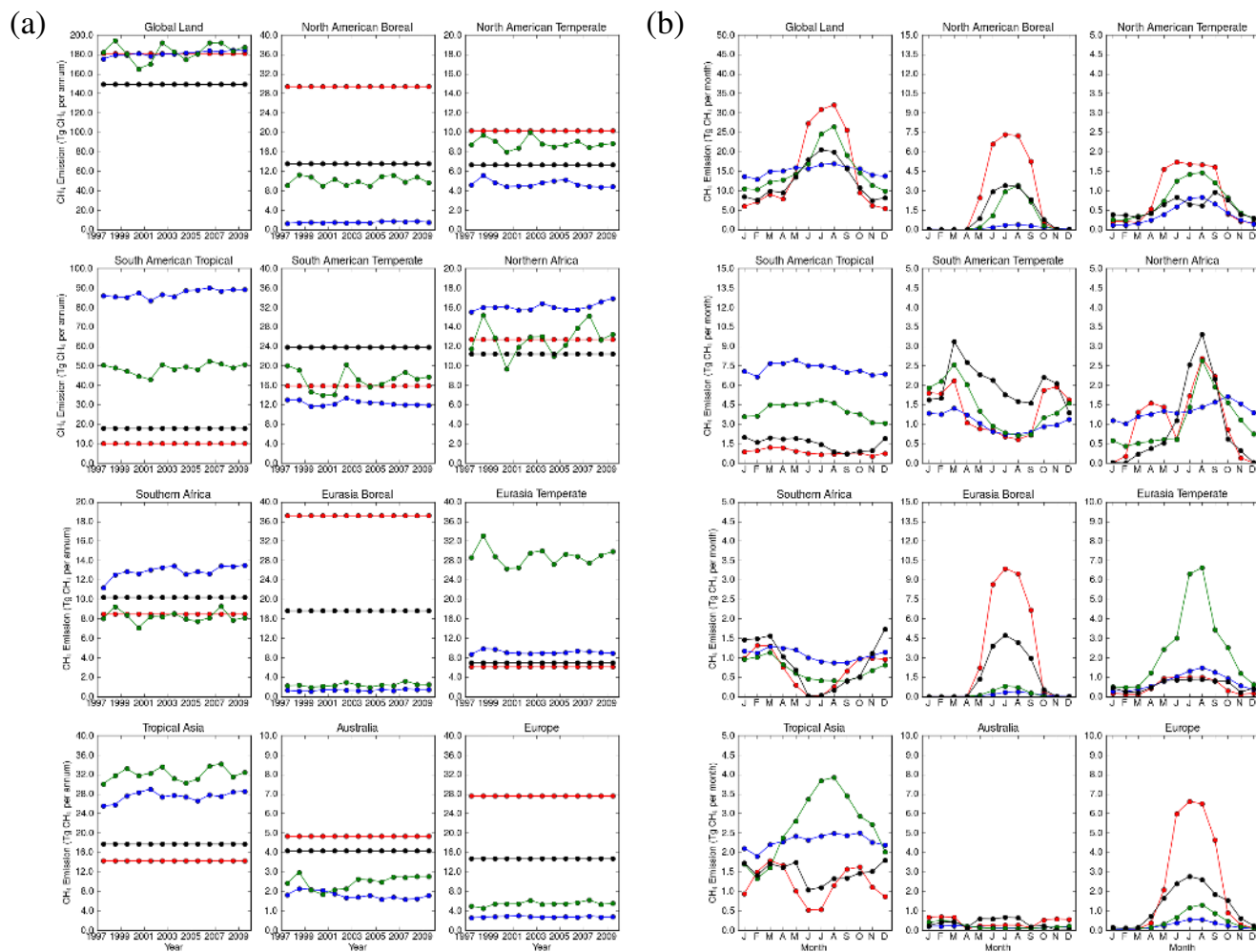
(a)

(b)

Figure 1. Time series of the area-weighted annual wetland emissions for all land surface points and for the 11 terrestrial TRANSCOM regions (left-hand panel) for the Fung et al. (1991) wetland data sets (red: as used by O'Connor et al. (2014); black: TRANSCOM-FUNG) and for the JULES wetland estimates (blue: JULES; green: JULES-GIEMS). The right-hand panel shows the corresponding mean annual cycles.

annual methane emissions for the year 2000 for the four runs. The model runs all used the same previously derived initial conditions, which represented a spun-up atmosphere for the early 2000s.

3.1 Comparison with surface measurements

We use the surface measurements of atmospheric CH_4 dry air mole fractions made at sites in the National Oceanic & Atmospheric Administration's Earth System Research Laboratory (NOAA ESRL) Carbon Cycle Cooperative Global Air Sampling Network (Dlugokencky et al., 2012). Section 2.1 in the Supplement includes a map of the monitoring sites and has time series of the observed and modelled atmospheric CH_4 concentrations between the years 2000 and 2010 at 16 of the 64 sites, covering both Northern Hemisphere (NH) and SH locations, for the different model runs. Figure 3 shows

a comparison of the latitudinal distribution of the observed monthly surface atmospheric methane mixing ratios from all the sites for the months of January, April, July and October (as a mean of the available measurements between 2000 and 2010) with the corresponding values derived from the four HadGEM2 runs. All four model runs reproduce the increase in methane mixing ratio between the SH and NH. The model runs also capture the variability (or lack thereof) in the NH (in the SH). The runs also reproduce the annual cycles observed at many of the SH sites.

There are differences in the modelled annual cycles at the NH sites for the four runs, which is more clearly seen in Fig. 4. The model run using the FUNG wetland emissions gives very high surface CH_4 concentrations and an incorrect seasonality at all the high- and mid-latitude NH sites (illustrated here by the Barrow, Pallas-Sammaltunturi and Mace Head sites). This has been seen by other authors (e.g. Patra
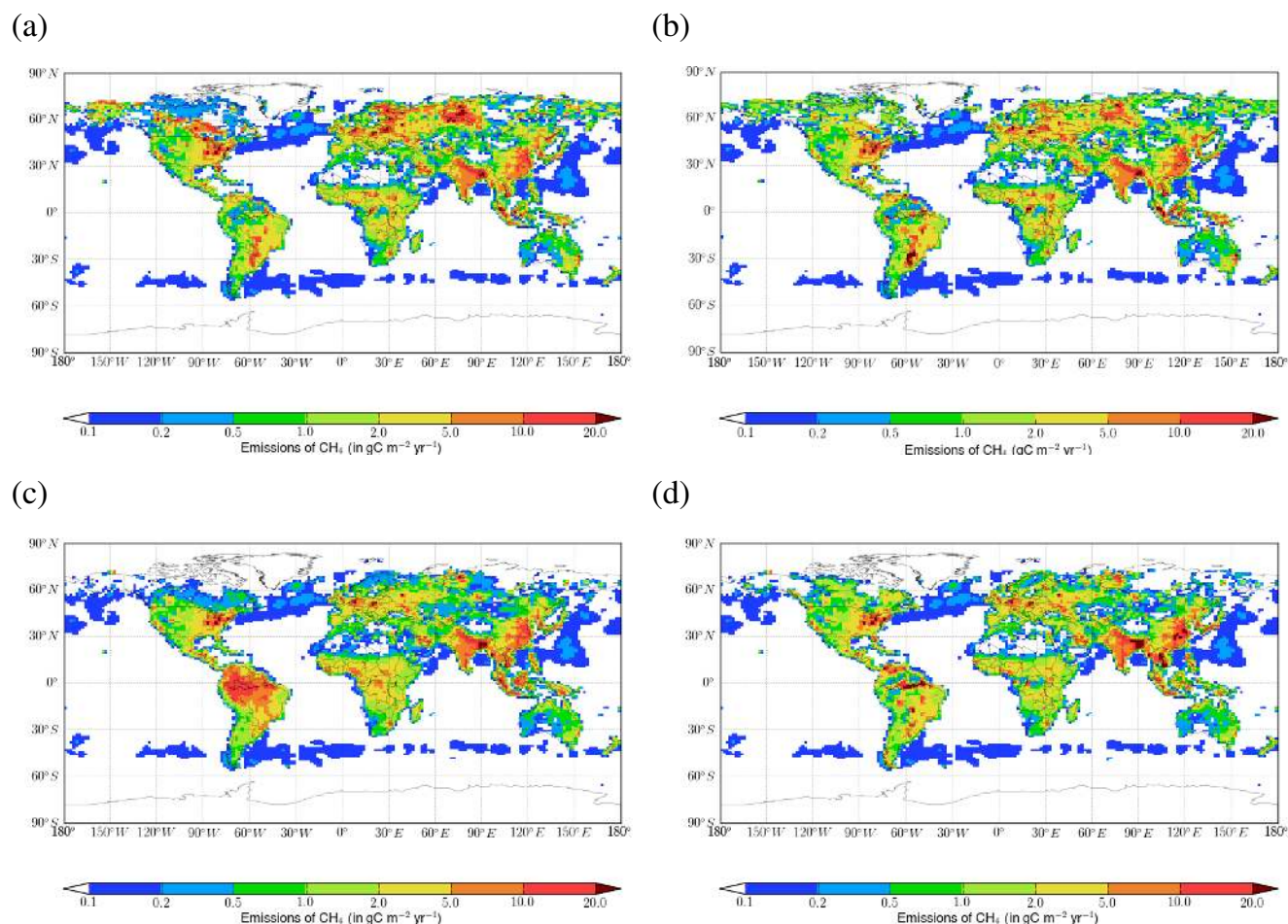
(a)

(b)

(c)

(d)

Figure 2. Maps of the global annual emissions of methane from all sources for the year 2000 using wetland emissions based on **(a, b)** the data set of Fung et al. (1991) (FUNG and TRANSCOM FUNG), **(c)** an offline JULES run (JULES) and **(d)** the same JULES run in which the modelled wetland fraction is replaced by that in the GIEMS product, corrected for rice paddy fields (JULES-GIEMS).

et al., 2011) and is also seen to a lesser extent in the run using the TRANSCOM-FUNG wetland inventory. The runs using the JULES wetland emission inventories are generally better in terms of amplitude and seasonality for these sites. We subsequently evaluate the model outputs using various metrics (see below). There is further evidence of the different spatial and temporal patterns between the wetland emission inventories at other mid-latitude NH sites (Hegyhatsal, Hungary; Ulaan Uul, Mongolia; Southern Great Plains, USA; and Plateau Assy, Kazakhstan). The modelled concentrations at the Arembepe site in Brazil provide evidence of the overprediction of the CH_4 emissions from the JULES wetland inventories. At many of the sites (e.g. Ulaan Uul, Mongolia; Southern Great Plains, USA; Tae-ahn Peninsula, Korea; Mount Waliguan, China; Mahe Island, Seychelles), the concentrations in the winter months are significantly overestimated, suggesting that the annual pattern of the non-wetland methane emissions may not be correct. The remote SH sites (illustrated here by the Tierra del Fuego and South Pole

sites) are located a long distance from the large CH_4 sources (which are mainly in the NH) and are representative of the remote and well-mixed SH, although there is evidence of the higher SH wetland emissions in the JULES and JULES-GIEMS runs.

The HadGEM2 configuration used for these runs does not provide "tagged" or "coloured" outputs (i.e. the contribution of the different methane source sectors cannot be derived). Instead, we estimate the contribution from the various source sectors (anthropogenic, rice paddy fields, shipping, wetlands, biomass burning, termites and oceanic/hydrates) using the sector emissions local to that region. In Table 4 of the Supplement, we present the relative contribution of the emissions sectors for a $20° \times 20°$ box centred on the Barrow and Plateau Assy sites. At Barrow, the emissions in the TRANSCOM-FUNG run are mainly from wetlands ($>62\%$), whereas the wetland emissions are smaller in the JULES and JULES-GIEMS runs and the emissions from anthropogenic sources make the largest contribution. A similar
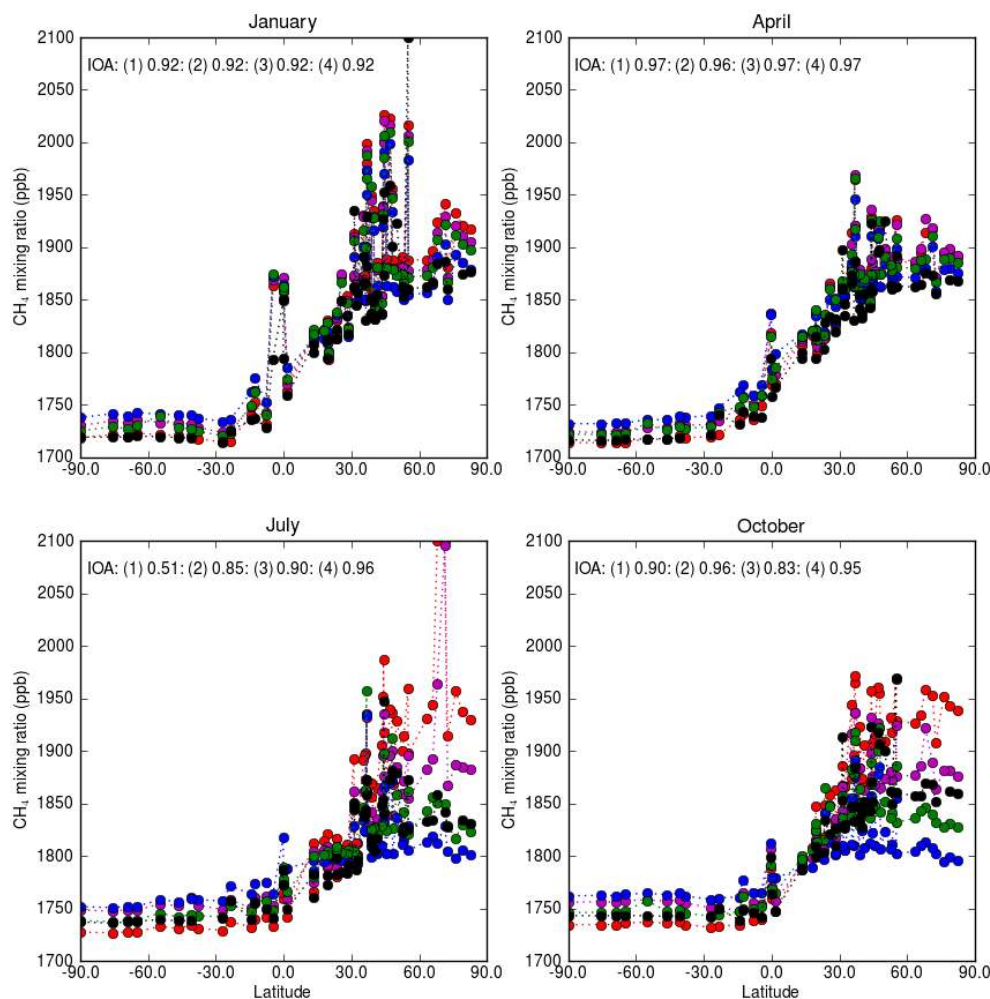
Figure 3. Comparison of the latitudinal distribution of the surface atmospheric methane mixing ratio (in ppb) as observed (black) and from the HadGEM2 runs using the following wetland emission inventories, (1) FUNG (red), (2) TRANSCOM-FUNG (magenta), (3) JULES (blue), and (4) JULES-GIEMS (green) between the years 2000 and 2010 for the months January, April, October and December. The index of agreement (IOA) is shown for each run (see Sect. 3 of the Supplement for the definition of the IOA).

pattern is also observed at the Pallas-Sammaltunturi site. At the Plateau Assy site, anthropogenic emissions are the largest contributing sector with wetlands at 25–29 % (TRANSCOM-FUNG), 0.3–6.0 % (JULES) and 11–13 % (JULES-GIEMS).

A wide variety of methods have been developed within the atmospheric composition and air pollution community to assess model performance (e.g. Yu et al., 2006; Dennis et al., 2010). For each of the HadGEM2 runs, we derived these different metrics (linear regression, bias, normalized mean bias, IOA, hit rate – see Sect. 3 in the Supplement) for each site where there were at least 20 pairs of monthly observed and modelled concentrations. The valid data from all sites for a given run were then aggregated and the same set of metrics derived for this "global" data set. Table 1 provides the output of this analysis. There are some remarkably good fits with slopes close to unity and high correlation coefficients ($R^2 = 0.82$ for the JULES-GIEMS inventory). That

said, there are specific sites where the performance appears superficially good but is less robust on closer inspection (see Table 6 in Sect. 2.1 of the Supplement). This can also be seen in Fig. 5, which shows a Taylor plot (Taylor, 2001) for the four runs (FUNG, TRANSCOM-FUNG, JULES and JULES-GIEMS). The JULES-based inventories represent an improvement over the FUNG and, to a lesser extent, the TRANSCOM-FUNG wetland inventories, where a negative correlation between the observed and modelled concentrations at high-latitude NH sites is evident for the latter. The index of agreement (and, to a lesser extent, the hit rate) did show some discrimination between the model runs. The IOA varies between 0.76 (FUNG) and 0.94 (JULES-GIEMS), the run in which the JULES-modelled wetland fraction is replaced with the EO-derived value. The run using the JULES-modelled wetland fraction gave an IOA of 0.91, showing that the JULES-based emission inventories are, in general, a con-
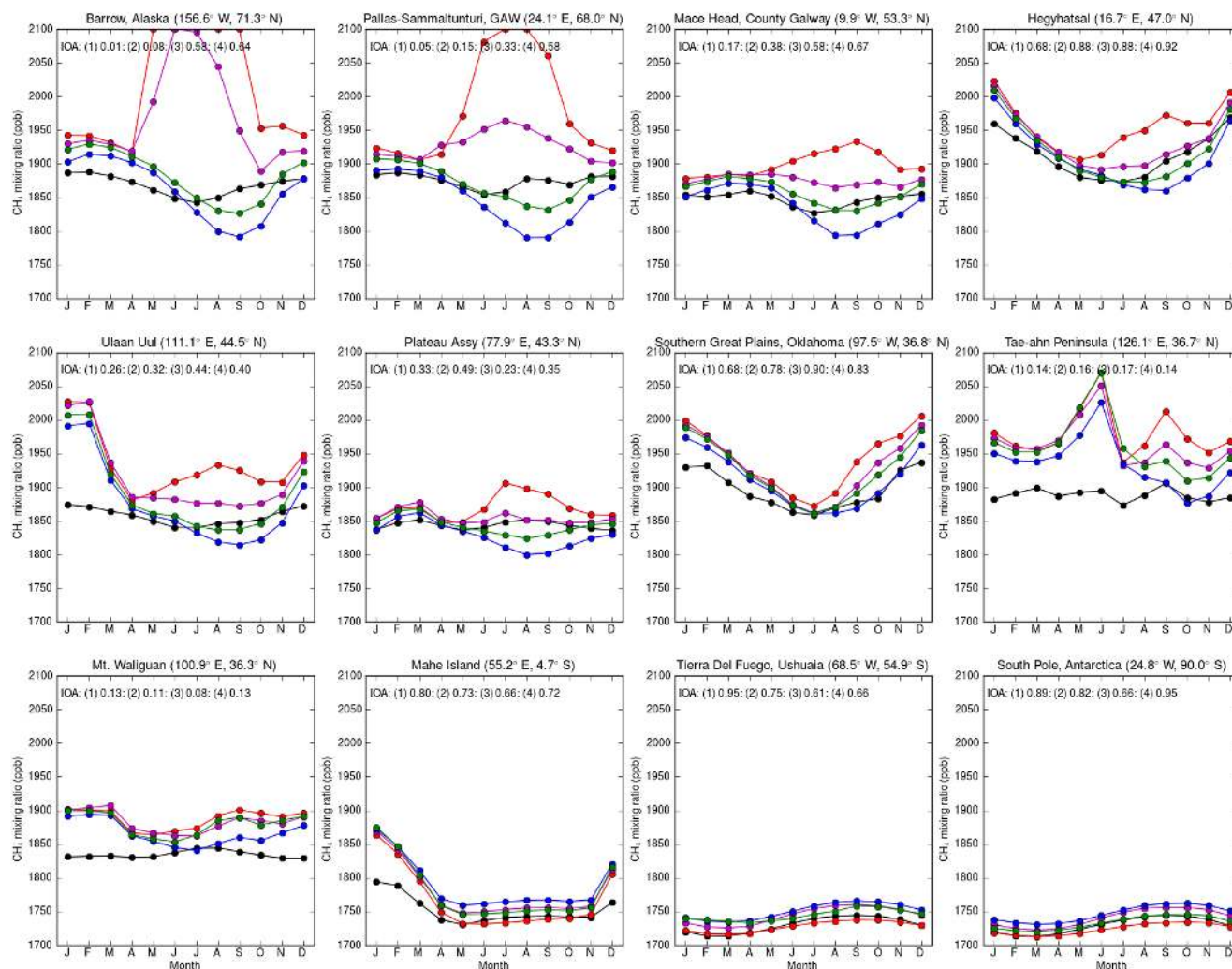
Figure 4. Comparison of the annual cycle in the surface atmospheric methane mixing ratio (in ppb) at selected sites between the years 2000 and 2010, as observed (black) and from the HadGEM2 runs using the following wetland emission inventories, (1) FUNG (red), (2) TRANSCOM-FUNG (magenta), (3) JULES (blue), and (4) JULES-GIEMS (green). The IOA is shown for each run.

siderable improvement over the run using the FUNG inventory (but not the run using TRANSCOM-FUNG inventory, for which an IOA of 0.91 is derived).

Of more relevance is whether the model can reproduce the observed growth rates and hence explain the origin of the positive anomalies. Following Dlugokencky et al. (1994a) and references therein, the average trend and seasonal cycle in the modelled or observed concentrations were approximated by a second-order polynomial and four harmonics. A low-pass filter was then applied to the residuals of the fit to remove variations occurring on timescales less than ~ 1 year. The smoothed residuals were added to the quadratic portion to give a deseasonalized trend. The growth rate was derived as the derivative of the monthly concentrations of this deseasonalized trend. Figure 6 shows the growth rates derived from the observed and calculated surface concentrations at six sites (Alert, Niwot Ridge, Mauna Loa, Ascension Island,

Bukit Kototabang and South Pole) for all the runs. The modelled growth rates are similar to each other and generally larger than those observed, reflecting the generally larger modelled annual cycles (see figures in Sect. 2.1 of the Supplement). It is less clear that the JULES-based inventories are generally better. The correspondence at many sites is variable and there is some indication that the modelled changes are more rapid than those observed.

3.2 Comparison with SCIAMACHY measurements

3.2.1 Initial comparison

We convert the modelled 4-D methane mass mixing ratio fields (longitude, latitude, altitude, time) into 3-D fields (longitude, latitude, time) of the mean dry-air atmospheric column methane mixing ratio, using the SCIAMACHY averag-

Table 1. Statistical outputs from the "global" analysis of the observed and modelled surface methane concentrations for the HadGEM2 runs (FUNG, TRANSCOM-FUNG, JULES and JULES-GIEMS) using valid co-located data from all monitoring sites.

| Statistic/Metric	FUNG	TRANSCOM-FUNG	JULES	JULES-GIEMS
Number of valid data pairs	5591	5591	5591	5591
Linear regression – slope	1.33	1.09	0.79	0.99
Linear regression – intercept	−563.3	−130.8	391.6	30.8
Coefficient of determination (R^2)	0.58	0.81	0.71	0.82
Mean of observations (in ppb)	1816.4	1816.4	1816.4	1816.4
Mean of modelled conc. (in ppb)	1849.8	1839.1	1820.9	1828.9
Mean normalized bias	0.02	0.01	0.003	0.01
Number of modelled results within a factor of 2	1.0	1.0	1.0	1.0
Index of agreement	0.76	0.91	0.91	0.94
Hit rate	0.93	0.97	0.99	0.98
Root mean square error (RMSE, in ppb)	78.4	38.7	33.0	30.8
Coefficient of variation in RMSE	0.04	0.02	0.02	0.02
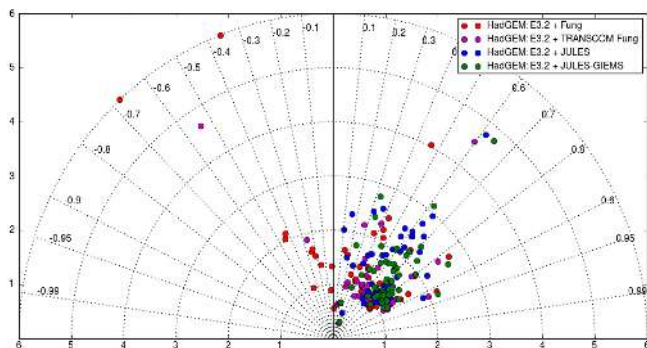
Figure 5. Taylor plot derived from the observed surface atmospheric methane mixing ratio (in ppb) and the HadGEM2 runs using the following wetland emission inventories, FUNG (red), TRANSCOM FUNG (magenta), JULES (blue) and JULES-GIEMS (green), for all valid data pairs from all sites.

ing kernels (Schneising et al., 2009). We then derive contour maps of the mean atmospheric mixing ratios of methane from the HadGEM2 model runs and the regridded version of the SCIAMACHY product (v2.3, Sect. 2.2.2) for the period 2003 to 2007. The model outputs are only sampled at the valid space and time points present in the SCIAMACHY product and a land–sea mask is applied to remove all data over the oceans as the SCIAMACHY data set only includes measurements over the oceans for the period between 2003 and 2005. As shown in Fig. 19 in the Supplement, there is a clear underprediction in the modelled atmospheric column methane mixing ratios by ~ 50 ppb (i.e. $\sim 3\%$ of a typically observed mean column mixing ratio).

We attribute the underprediction to a faster fall-off in modelled methane concentrations with altitude than that observed. To test this, we initially replaced the HadGEM2 model outputs above 400 hPa with methane mixing ratios derived from the thermal infrared (TIR) channel of the Tropospheric Emission Spectrometer (TES, AURA, 2004–

2011: Beer, 2006), because of its availability and ease of use. As discussed by Worden et al. (2012), the CH$_4$ in the upper troposphere is biased high relative to the lower troposphere by 4% on average. Given this and the poor temporal overlap with the SCIAMACHY data set, we subsequently constrained the HadGEM2 output above 300 hPa with data from HALOE/ACE-assimilated TOMCAT output (see Sect. 2.2.3), which covered the entire period of the HadGEM2 runs (2000–2007) and the SCIAMACHY measurements. Figure 7 shows a typical comparison of the HadGEM2 modelled vertical concentration profile of CH$_4$ with the corresponding profiles from TES and the HALOE/ACE-assimilated TOMCAT model for the grid square centred on the location (10° N, 1° E) in July 2005. The figure also shows the revised profiles derived by replacing the HadGEM2 modelled concentrations with interpolated TES measurements (above 400 hPa) and the HALOE-assimilated TOMCAT output (above 300 hPa). The derived mean atmospheric methane column mixing ratios (in ppb) were: 1725.9 (HadGEM2, original), 1780.2 (HadGEM2+TES) and 1766.4 (HadGEM2+HALOE-TOMCAT), compared to the SCIAMACHY measurement of 1760.9 ppb.

O'Connor et al. (2014) introduce an explicit loss term in the standard tropospheric chemistry scheme to compensate for the lack of CH$_4$ oxidation in the stratosphere. However, the faster fall-off with height cannot be attributed to this additional explicit loss term (see Sect. 2.1.2). In the model runs carried out here, although the global annual loss rate of stratospheric CH$_4$ is higher than previous estimates (53 ± 4 Tg CH$_4$ yr^{-1} compared to 40 Tg CH$_4$ yr^{-1} from Prather et al. (2001)), similar behaviour has been seen in the stratospheric configuration of UKCA (Morgenstern et al., 2009). Given the different treatment of stratospheric CH$_4$ removal in the two UKCA configurations and that stratospheric chemical removal rates are much slower than transport timescales (Zahn et al., 2006), it is likely that the faster fall-off of modelled stratospheric CH$_4$ with height than
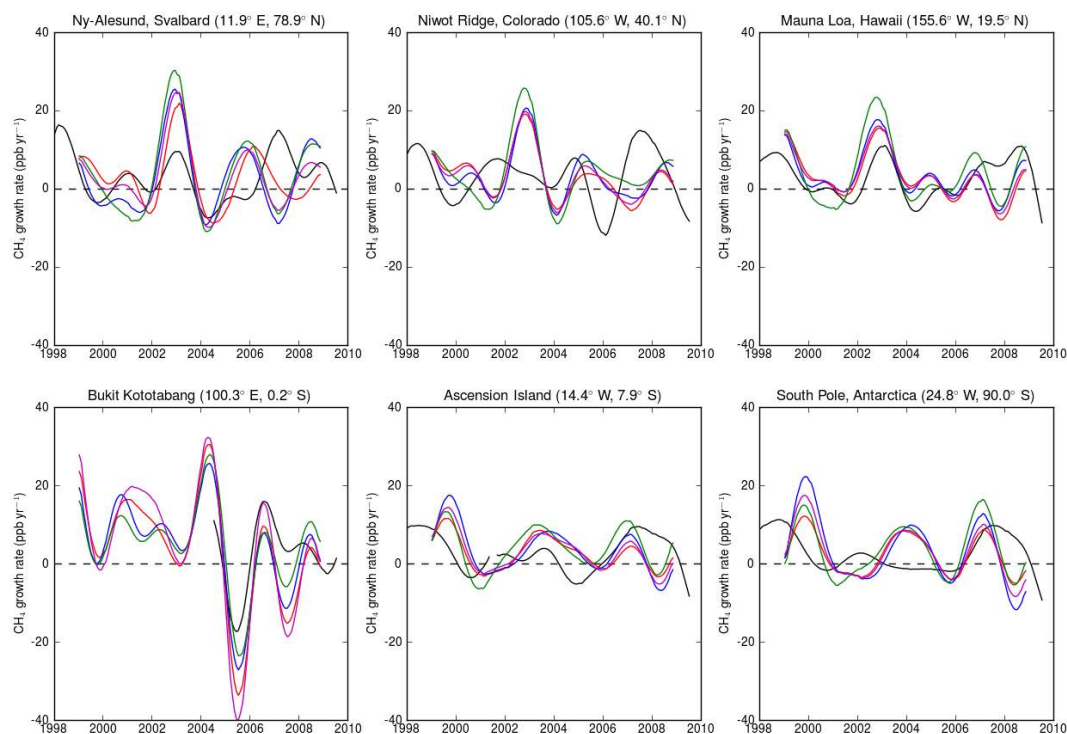
Figure 6. Comparison of the growth rates in the surface atmospheric methane mixing ratio (in ppb) as observed (black) and from the HadGEM2 runs using the following wetland emission inventories, FUNG (red), TRANSCOM FUNG (magenta), JULES (blue) and JULES-GIEMS (green) at selected sites between the years 1998 and 2010.
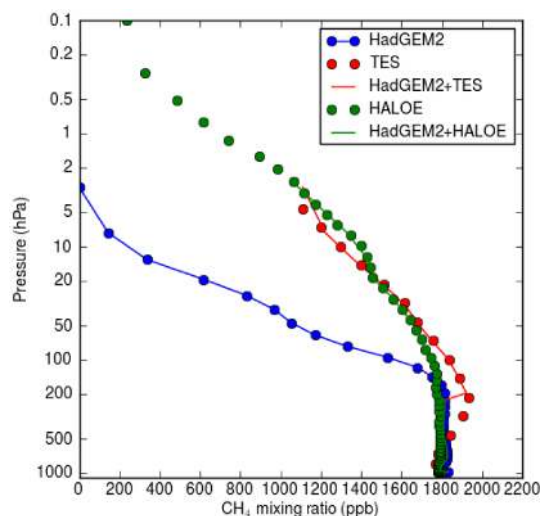

Figure 7. Comparison of the HadGEM2 modelled vertical concentration profile of CH_4 with the corresponding profiles from the TES (red) and the HALOE-assimilated TOMCAT model for the grid point (10° N, 1° E) in July 2005. The red and green lines show the results from replacing the HadGEM2 modelled concentrations above 200 hPa with TES and the HALOE-assimilated TOMCAT output, respectively.

that observed is an indication that stratospheric transport timescales are too long.

Constraining the modelled CH_4 concentrations at model levels above 300 hPa improved the agreement with the SCIA-MACHY SWIR CH_4 product (Fig. 19 in the Supplement). All subsequent comparisons with the SCIAMACHY product are based on the merged HadGEM2 and HALOE/ACE-assimilated TOMCAT outputs. As our emphasis is on testing different wetland CH_4 emission configurations, this extra constraint being applied to HadGEM2 output is appropriate.

3.2.2 Comparisons in space and time

Figure 8 compares the mean atmospheric column measurements of methane derived from the regridded SCIAMACHY product for the period 2003–2007 and the HadGEM2 runs using the FUNG, TRANSCOM-FUNG, JULES and JULES-GIEMS methane wetland emission inventories, constrained as described in the previous section. We note that (i) the model reproduces the latitudinal gradient in the atmospheric methane column, with higher methane columns in the NH; (ii) the model captures the high emission areas over south and south-east Asia, although the modelled concentrations are much higher than those observed; (iii) the different spatial patterns of the wetland methane emissions used are evident in the maps. We see enhanced atmospheric columns over the boreal Eurasia region in the run using the FUNG wetland in-
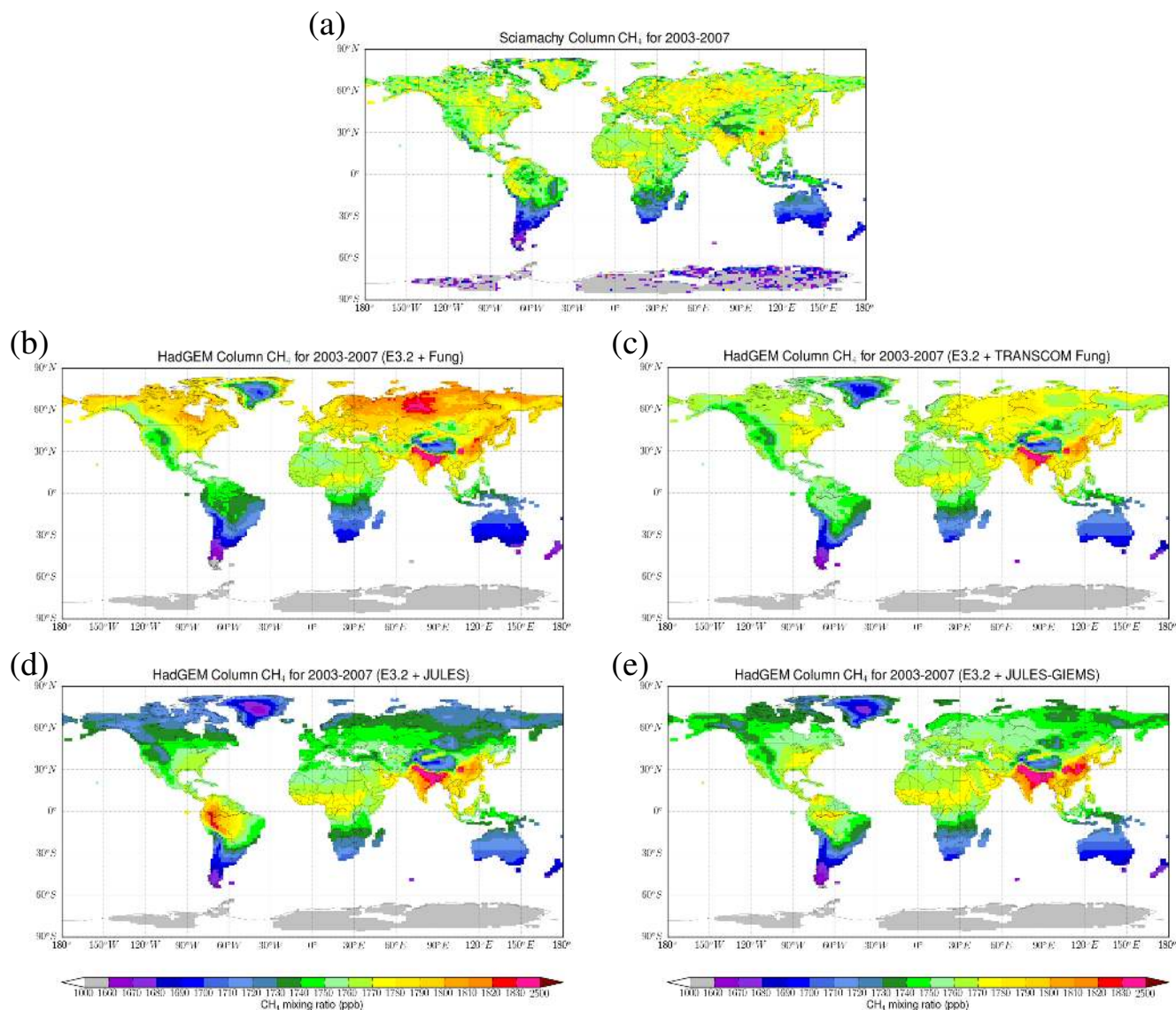
(a)

(b) (c) (d) (e)

Figure 8. Contour maps of the average atmospheric column methane mixing ratio between the years 2003 and 2007, as derived from monthly regridded SCIAMACHY data **(a)** and from the HadGEM2 runs using the FUNG **(b)**, TRANSCOM-FUNG **(c)**, JULES **(d)** and JULES-GIEMS **(e)** wetland emission inventories and the EDGAR v3.2 (E3.2) anthropogenic methane emission time series, sampled at co-located space and time points.

ventory and over the Amazon in the run using the JULES wetland inventory.

We compare the latitudinal distributions in Fig. 9. The run using the TRANSCOM-FUNG wetland inventory gives a remarkably good description. The larger emissions present at temperate and higher NH latitudes in the FUNG wetland inventory result in higher zonal averages at these latitudes compared to both TRANSCOM-FUNG and the JULES-based inventories. The JULES-based inventories give better agreement in the tropics and SH compared to the FUNG inventory but underestimate the atmospheric column at boreal and higher northern latitudes. The high modelled mixing ratios

over the Ganges Valley in India are evident in the peaks in the modelled profiles between 20 and 30° N in all four runs.

Figure 10 shows time series and annual cycles of the area-weighted mean atmospheric column methane mixing ratios between January 2003 and December 2007 from the SCIAMACHY data and the four HadGEM2 runs for all land surface points and for the 11 terrestrial TRANSCOM regions (see map at http://transcom.project. asu.edu/transcom03_protocol_basisMap.php). In Fig. 20 in the Supplement, we include similar time series and annual cycle plots using the unconstrained HadGEM2 model outputs. We know that the FUNG wetland emission inventory
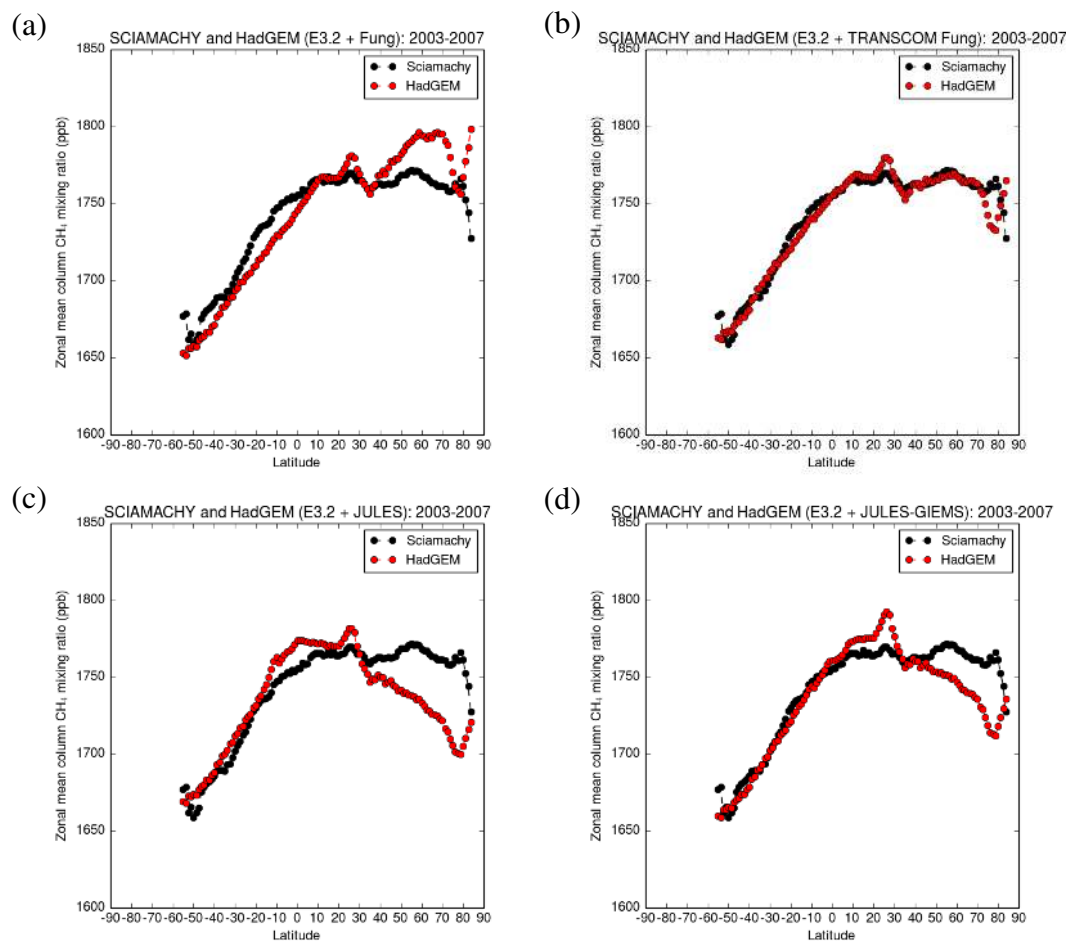
Figure 9. Comparisons of the latitudinal distribution of the average atmospheric column methane mixing ratio between the years 2003 and 2007, as derived from monthly regridded SCIAMACHY data and from the HadGEM2 runs using the FUNG **(a)**, TRANSCOM-FUNG **(b)**, JULES **(c)** and JULES-GIEMS **(d)** wetland emission inventories and the EDGAR v3.2 (E3.2) anthropogenic methane emission time series, sampled at co-located space and time points. Note that the SCIAMACHY data between 60 and 90° S have been removed because of their sparsity and quality.

used here gives too much emission at boreal and higher latitudes. This is apparent from the very strong annual cycles with summer maxima (30–50 ppb enhancements) for Europe and the two boreal zones in North America and Eurasia. The run using TRANSCOM-FUNG wetland inventory also has annual cycles with summer maxima for Europe and the two boreal zones in North America and Eurasia. The JULES-based inventories, on the other hand, show summer minima, similar to the behaviour seen in the surface measurement sites (see Fig. 4). It is also evident that the monthly emission profiles of some source sectors appear incorrect. In the Tropical Asia region, the annual cycle shows a minimum in July for all four runs whereas the SCIAMACHY data show a maximum in the late summer/early autumn. Also included in each panel of Fig. 10 are the IOAs derived for the four HadGEM2 runs. As presented, the values generally show that the model run using the FUNG wetland emission inventory performed the best when all land surface points are considered together

(IOA = 0.86) and for some of the TRANSCOM regions in the Northern Hemisphere. However, the JULES-based inventories were better in the SH (e.g. IOA for JULES-GIEMS = 0.59 for South American Temperate, Southern Africa and Australia). The high modelled mixing ratios over the Ganges Valley in India, evident in Figs. 8 and 9 in all four runs, occur in the winter months. This suggests that the stronger summer emissions in the FUNG wetland emission inventory compensate for the lack of or opposite seasonality in the emissions from other source sectors (see Figs. 4–7 in the Supplement).

3.3 Discussion

3.3.1 Comparison against measurements

The comparison of the model outputs against the in situ surface atmospheric and atmospheric column measurements of
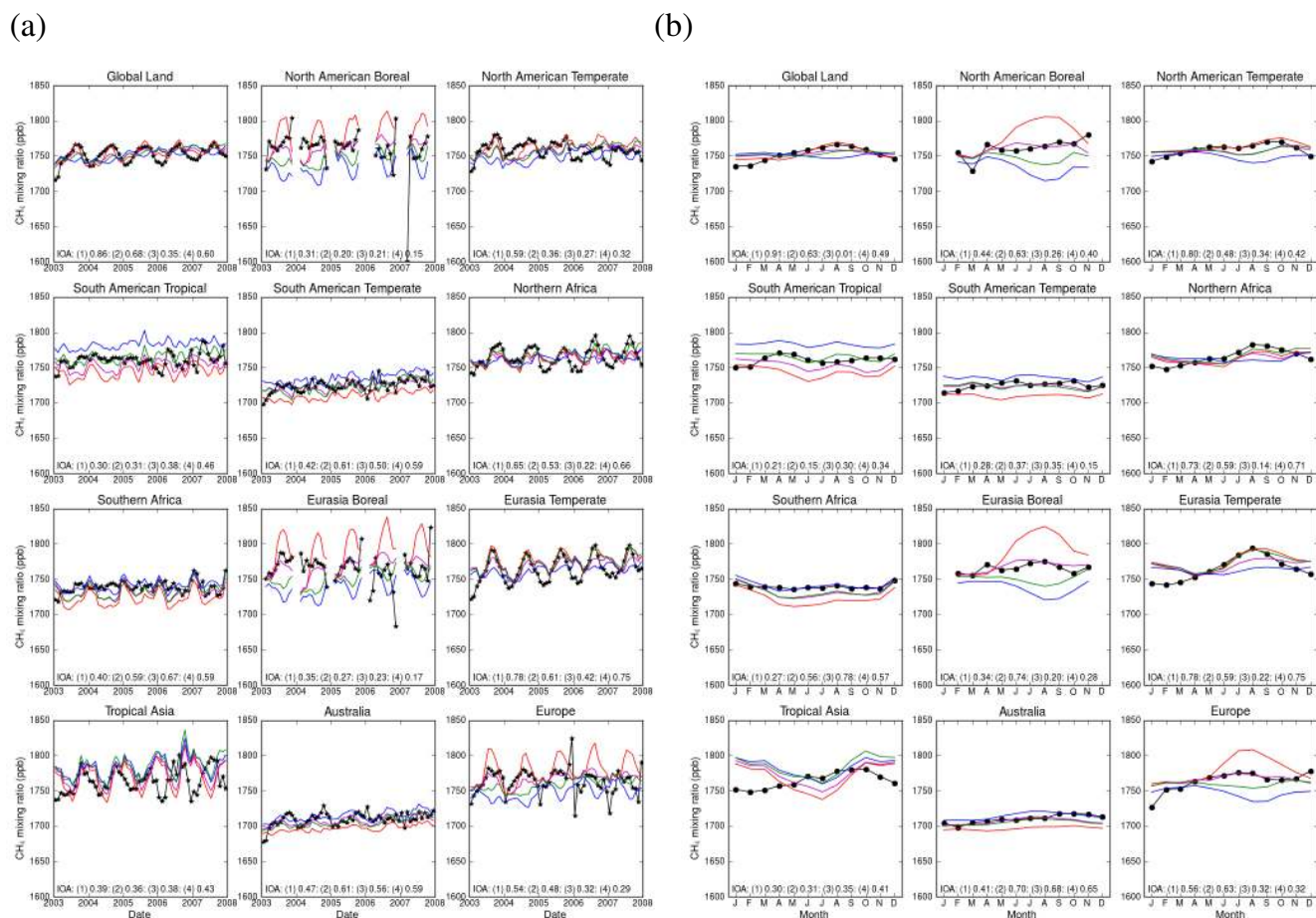
(a)

(b)

Figure 10. Time series of the area-weighted average atmospheric column methane mixing ratio from January 2003 to December 2007, as derived from monthly regridded SCIAMACHY data (v2.3) and from the HadGEM2 runs using (1) the FUNG (red), (2) the TRANSCOM FUNG (magenta), (3) the JULES (blue), and (4) the JULES-GIEMS (green) wetland emission inventories and the EDGAR v3.2 (E3.2) anthropogenic methane emission time series, sampled at co-located space and time points for all land surface points and for the 11 terrestrial TRANSCOM regions **(a)**. **(b)** shows the corresponding annual cycles. The IOA is shown for each run (see Sect. 3 of the Supplement for the definition of the IOA).

methane has indicated varying levels of agreement. The run using the JULES-GIEMS wetland emission inventory gives the best description of the surface observations and the derived growth rates. The observed growth rates clearly show the positive anomalies in 1997/1998 and 2002/2003 and the increase in methane after 2007 (see Fig. 6). The model captures these events with varying degrees of success. There is also evidence from the high-latitude SH sites that the modelled atmospheric burden is increasing too quickly.

We expect the in situ surface atmospheric measurements to be more sensitive to the methane emissions, whereas the atmospheric column measurements integrate the effects of emissions, chemistry and atmospheric transport. The large amplitudes seen in the annual cycles of the in situ surface atmospheric observations (Fig. 4), especially at the high NH latitude sites, are less apparent in the modelled atmospheric columns, possibly because of the limited number of SCIA-

MACHY observations at these latitudes, and the model outputs were only sampled if there was a valid SCIAMACHY measurement. Figure 10 and Fig. 20 in the Supplement show comparisons of the observed SCIAMACHY and modelled time series and annual cycles for the constrained and unconstrained HadGEM2 model outputs, respectively. The amplitudes of the annual cycles appear larger in the unconstrained model outputs, especially the FUNG and TRANSCOM-FUNG runs, as these effectively have larger contributions from the model levels close to the surface and these levels are more affected by the surface emissions. Generally, we see similar trends and patterns between the constrained and unconstrained model outputs, suggesting that the different emission distributions largely account for the differences in the modelled atmospheric concentrations and columns between the model runs.
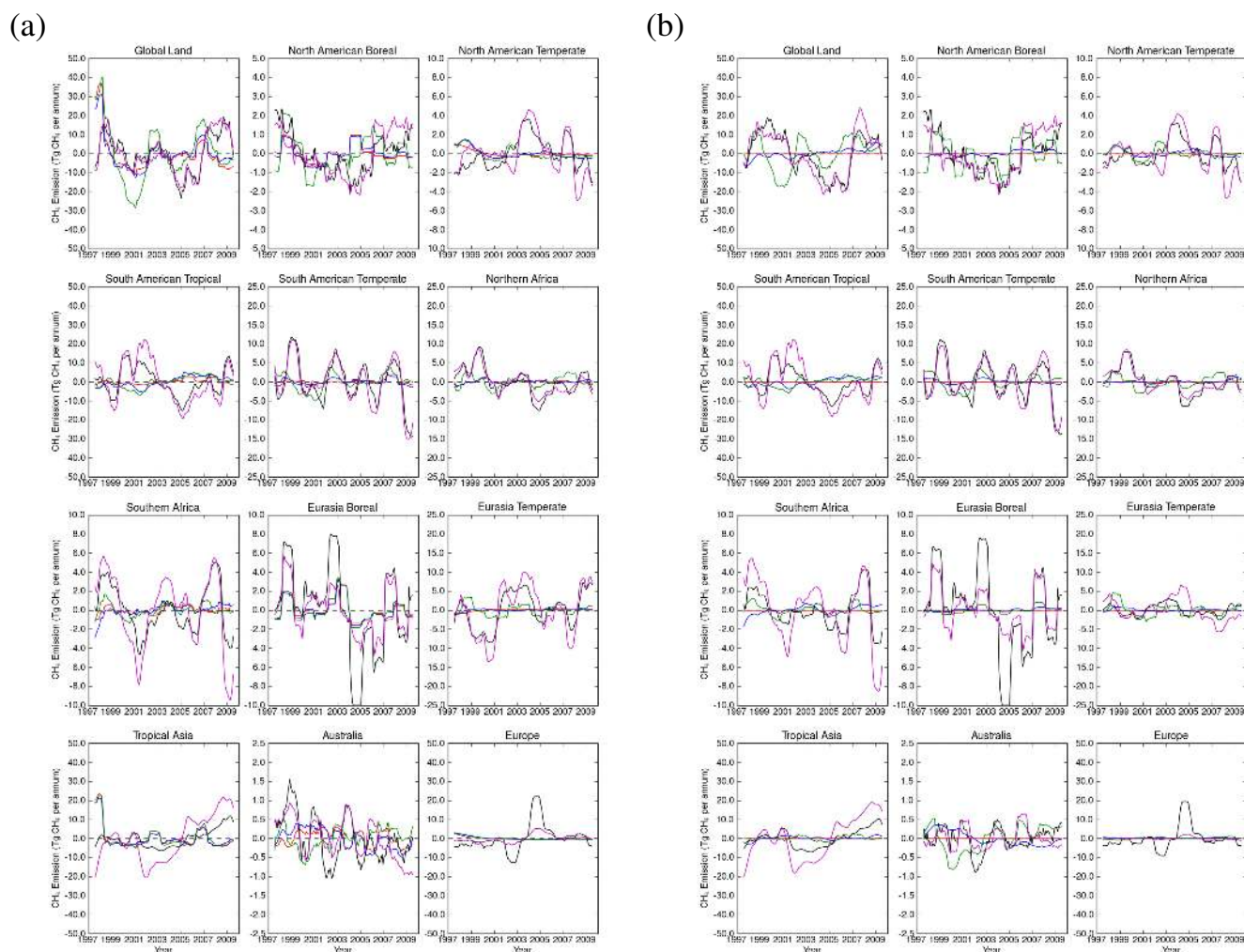
(a)

(b)

Figure 11. Comparison of the deseasonalized emission fluxes between 1997 and 2009 from the HadGEM2 runs (using the wetland emission inventories: FUNG – red, JULES – blue and JULES-GIEMS – green) and the two inverse flux estimates of Bousquet et al. (2011) (black and purple). **(a)** and **(b)** show the anomalies in the global methane emissions and in the wetland emissions, respectively.

Compared to the SCIAMACHY observations, the constrained model run using the Fung-derived inventory appears better in terms of the annual cycle (Fig. 10), although its annual cycle in the boreal zone is larger. The JULES-based inventories on the other hand exhibit a smaller seasonal cycle (for the JULES inventory, this is because the wetland emissions are dominated by those from the Amazon and these are modelled to have little seasonality). The high concentrations modelled over the Ganges in India in all four runs indicate that the magnitude of the non-wetland emissions in this region and their monthly variability may be too large (see Fig. 9) or that the boundary layer mixing in this region, close to the Himalayan mountains, is not well represented. There is evidence in the comparison with the inverse emission estimates that part of the explanation is that the emissions are overstated in this region (and these are largely CH_4 emissions from non-wetland sources). Further support for this interpre-

tation is provided by Patra et al. (2009), who found that the methane emissions from India were lower by 13 $Tg\,CH_4\,yr^{-1}$ in their optimized emission scenario.

3.3.2 Comparison with other wetland estimates

Wetlands are generally accepted as being the largest, but least well quantified, single natural source of CH_4 (Denman et al., 2007; USEPA, 2010). In this work, the mean annual global emission between 1999 and 2007 was effectively fixed at 181 $Tg\,CH_4\,yr^{-1}$, the value used by O'Connor et al. (2014) in earlier HadGEM2 model runs. The total is however consistent with other recent estimates. Bousquet et al. (2011) derived a value of 165 $Tg\,CH_4\,yr^{-1}$ from their inverse modelling study. Melton et al. (2013) reported an ensemble mean of the annual global emissions of 190 $Tg\,CH_4\,yr^{-1}$ with a spread of $\pm 40\%$ from the wetland models partici-

Table 2. Comparison of global and regional estimates of methane emissions from wetlands.

Domain	Model/Observation-based estimate (Ref.)	JULES (1997–2009)	JULES-GIEMS (1997–2009)	FUNG (as used here)	TRANSCOM/ FUNG
Global	(TD: 2000s) 175 (142–208) (1)				
	(BU: 2000s) 217 (177–284) (1)	181 (178–184)	181 (167–194)	181	149
Global – WETCHIMP	190 (141–264) (2)				
Boreal (> 30° N)	37.7–157.3 (3)	12.6 (12.2–13.2)	35.1 (32.8–37.4)	109	58.5
Hudson Bay Lowlands	2.3 ± 1.3 (4)	0.4 (0.3–0.6)	2.2 (1.8–2.6)	10.2	3.5
West Siberian Lowlands	2.93 ± 0.97 (5)	0.5 (0.4–0.6)	1.6 (1.3–2.2)	19.1	8.0
Tropics (23° S–23° N)	111.1 (6)	159 (157–162)	123 (112–134)	57.3	69.4
Amazon	26.6 (6)	89 (85–91)	53 (46–59)	17	25
Amazon (Nov 2008)	3.3 (1.5–4.8) (7)	5.7	2.2	1.2	1.4
Amazon (May 2009)	3.3 (1.3–5.5) (7)	6.5	3.9	0.6	1.4

Notes: For the JULES and JULES-GIEMS wetland inventories, we show the mean (minimum–maximum) annual emission of the years 1999–2007. The JULES-GIEMS wetland inventory was corrected for the area of rice paddy fields, as described in Sect. 2.3.1.
References: (1) top–down (TD) and bottom–up (BU) wetland emission estimates for the 2000s taken from Kirschke et al. (2013); (2) taken from the WETCHIMP wetland model intercomparison of Melton et al. (2013); (3) range of emission estimates from Petrescu et al. (2010) using the PEATLAND-VU wetland CH_4 emission and PCR-GLOBWB hydrological models, driven with different wetland data sets; (4) Pickett-Heaps et al. (2011), domain taken to be 96–75° W and 50–60° N; (5) version (Bc8) of the "standard model" in Glagolev et al. (2011), domain taken to be 65–85° E and 54–70° N; (6) Bloom et al. (2012), the wetland emissions from the Amazon are 24 % of the total wetland emissions from the tropics; (7) mean (range of) emission estimates for Amazon Lowlands for November 2008 and May 2009 from Beck et al. (2013).
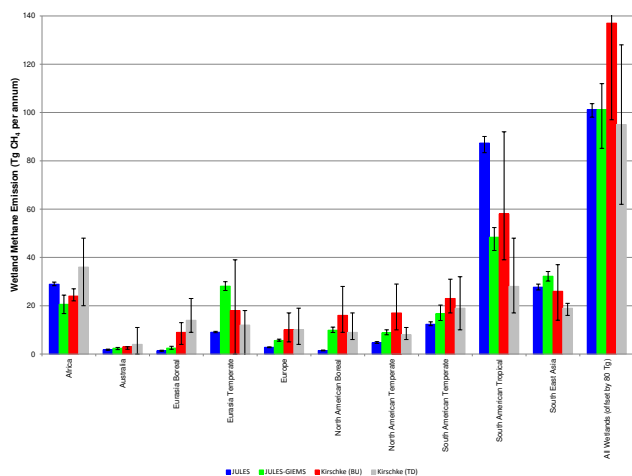

Figure 12. Mean annual methane emissions for the period 2000–2009 from the JULES (blue) and JULES-GIEMS (red) used in this work and the bottom–up (green) and top–down (grey) estimates of Kirschke et al. (2013). The "all wetlands" components have been offset by $80\,Tg\,CH_4\,yr^{-1}$ for greater clarity. The error bars give the range of values.

pating in the WETCHIMP wetland model intercomparison. Fraser et al. (2013) obtained wetland emissions between 184 and $195\,Tg\,CH_4\,yr^{-1}$ from inversions of surface and/or GOSAT measurements between 2009 and 2010. In a synthesis paper, Kirschke et al. (2013) estimated methane emissions from natural wetlands for the period 2000–2009 to be in the range from 142 to $208\,Tg\,CH_4\,yr^{-1}$ with a mean value of $175\,Tg\,CH_4\,yr^{-1}$ using inverse modelling methods and in the range from 177 to $284\,Tg\,CH_4\,yr^{-1}$ with a mean value of $217\,Tg\,CH_4\,yr^{-1}$ from process-based approaches (see Table).

As the long-term mean annual emissions were fixed, the emphasis here has been on the spatial patterns and intra-annual and interannual variability. As shown in Fig. 2 in the Supplement, the JULES wetland emissions are concentrated in the tropics and especially the Amazon. The JULES-GIEMS still has more emissions in the tropics but these are located more in India and SE Asia (and a smaller increase in the Boreal emissions). In Table , we compare wetland emission estimates from JULES and JULES-GIEMS with other recent global and regional literature estimates. Petrescu et al. (2010) found a wide variation in methane emission fluxes from wetlands and floodplains above 30° N for the years 2001 to 2006 for different estimates of wetland extents (37.7
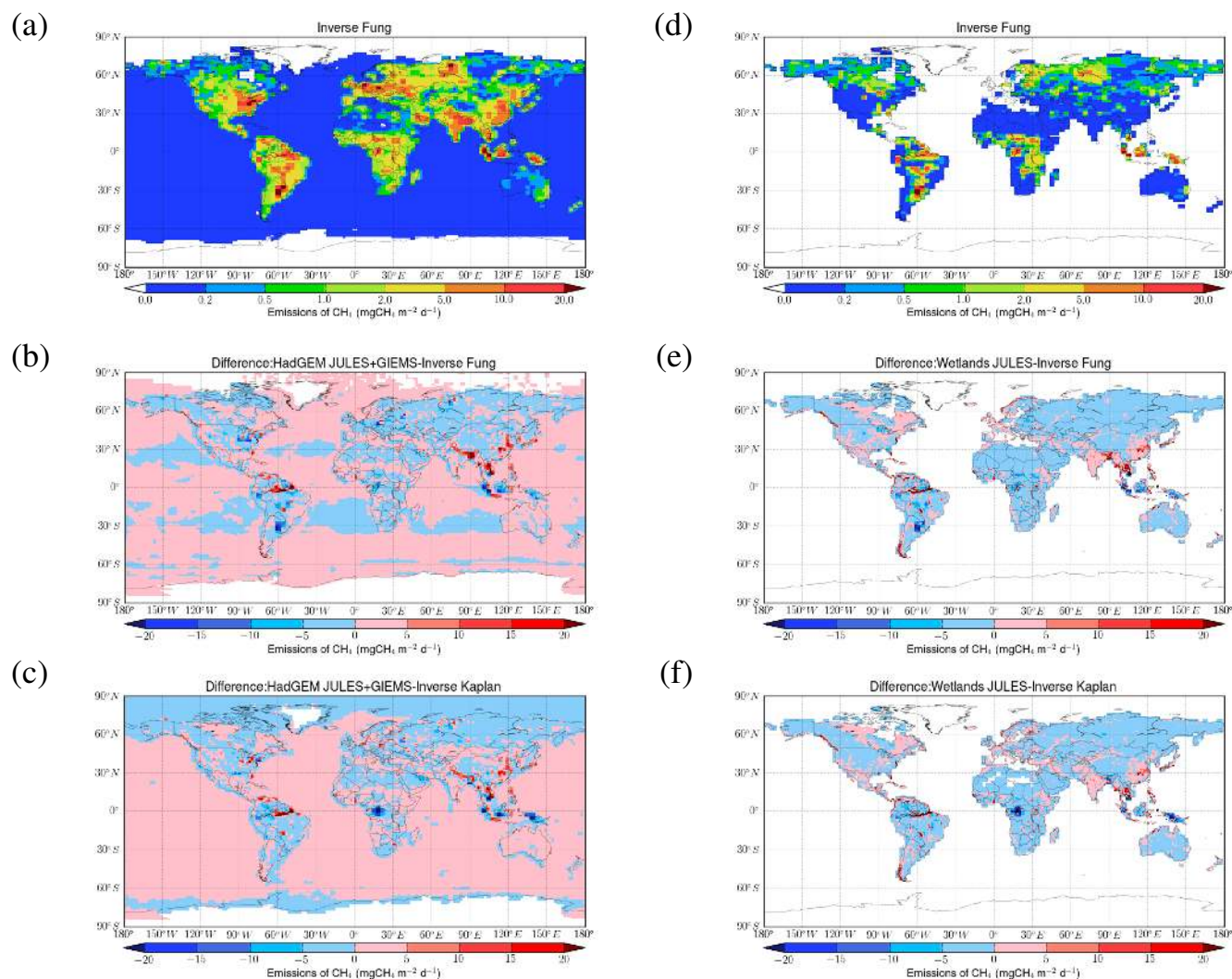
(a)

(d)

(b)

(e)

(c)

(f)

Figure 13. Annual methane emissions for 2000 from all sources (left-hand panels) and wetlands (right-hand panels). The upper panels **(a, d)** show the emission maps from the inverse modelling of Bousquet et al. (2011) using the data set of Fung et al. (1991) for the prior wetland emissions. Panels **(b)** and **(e)** show difference maps between the emission estimates shown in Panels **(a)** and **(d)** and the corresponding inventories using the JULES-GIEMS wetland emission inventory. Panels **(c)** and **(f)** are the same as Panels **(b)** and **(e)** but replacing the prior wetland emissions with those of Kaplan (as described in Bergamaschi et al., 2007).

to $157.3 \, \text{Tg CH}_4 \, \text{yr}^{-1}$). The corresponding JULES-GIEMS estimate for the same period is $35.1 \, \text{Tg CH}_4 \, \text{yr}^{-1}$, although we believe that this is an underestimate from the comparison against the atmospheric measurements. For the West Siberian Lowlands, Glagolev et al. (2011), using more measurement sites, revised the mapping-based estimate given by Kim et al. (2011) to $2.93 \pm 0.97 \, \text{Tg CH}_4 \, \text{yr}^{-1}$. The corresponding JULES estimates are lower, which we believe arises from the absence of peatland soils in JULES. There is better agreement for the JULES-GIEMS inventory with the estimate of Pickett-Heaps et al. (2011) for the Hudson Bay Lowlands. Bloom et al. (2010, 2012) report a 7% rise in global wetland CH_4 emissions over 2003–2007, due to warming of mid-latitude and Arctic wetland regions. Following the in-

troduction of a time decay of the substrate carbon to account for the observed seasonal lag between CH_4 concentrations and the peak in the equivalent water height, used as a proxy for a wetland, Bloom et al. (2012) derive revised global CH_4 emissions for 2003–2009. Tropical emissions amount to $111.1 \, \text{Tg CH}_4 \, \text{yr}^{-1}$, of which 24% is emitted from Amazon wetlands. As expected, the emissions in the tropics for 1999–2007 from the JULES and JULES-GIEMS inventories are higher, at $159 \, \text{Tg CH}_4 \, \text{yr}^{-1}$ (for the tropics with the Amazon accounting for $89 \, \text{Tg CH}_4 \, \text{yr}^{-1}$) and $123 \, \text{Tg CH}_4 \, \text{yr}^{-1}$ (with the Amazon contributing $53 \, \text{Tg CH}_4 \, \text{yr}^{-1}$), respectively. We see that the JULES-GIEMS inventory is in reasonable agreement with these regional estimates. The JULES–GIEMS inventory is also in good agreement with the emission esti-

mates obtained by Beck et al. (2013) for the Amazon Lowlands for November 2008 and May 2009. The JULES inventory again overestimates the emissions. In Fig. 12, we compare the regional emission totals given by the two JULES-based inventories with the corresponding information given in Kirschke et al. (2013) from their top–down and bottom–up approaches for the period 2000–2009. The comparison again indicates that the wetland emissions are too high in the Amazon for the JULES emission inventory and too low at boreal and higher latitudes. The JULES-GIEMS emission estimates are an improvement in that respect.

3.3.3 Comparison with inverse emission estimates

In Fig. 11 we compare the anomalies in the deseasonalized global and wetland methane emissions used in the HadGEM2 runs and from two inverse flux estimates derived by Bousquet et al. (2011) from surface atmospheric methane measurements, specifically, using prior wetland emission estimates based on Fung et al. (1991) and Kaplan (as described in Bergamaschi et al., 2007). The FUNG data set as used here shows no change in the anomaly of the wetland emissions as a single annual data set is used for all years; this is also the case for other methane sources, apart from biomass burning. Any anomalies in the emissions therefore largely result from biomass burning. The variability shown in the JULES model run is largely from the biomass burning – the wetlands show a steady increase. On the other hand, there is more interannual variability in the model run using the JULES-GIEMS wetland emission inventory. The inventories used here confirm other studies that link the 1997/1998 and the 2002/2003 positive growth anomalies in surface atmospheric methane concentrations to biomass burning (see Introduction, Dlugokencky et al., 2001; Simmonds et al., 2005). There is some suggestion from the JULES-GIEMS runs that wetland emissions contributed to the 2002/2003 anomaly (see Fig. 11).

The JULES inventory shows an upward trend over time while there is more interannual variability in the JULES emission data set driven with the EO inundation product (see Fig. 1). We compare the annual methane emission totals derived from the JULES-based estimates used here with two optimized inverse estimates of Bousquet et al. (2011). The mean (minimum–maximum) annual emissions between 1999 and 2007 are: JULES, 181 (178–184) $Tg\,CH_4\,yr^{-1}$; JULES-GIEMS, 181 (165–192) $Tg\,CH_4\,yr^{-1}$; Bousquet–Fung, 161 (143–180) $Tg\,CH_4\,yr^{-1}$; and Bousquet–Kaplan, 174 (156–198) $Tg\,CH_4\,yr^{-1}$. There is some agreement between the JULES-GIEMS and the inverse Bousquet–Kaplan emission inventories but also differences in the annual emission trends.

Figure 13 shows maps of the global annual emissions for the year 2000 for the inverse emission inventory estimates derived by Bousquet et al. (2011) using the wetland emission prior based on Fung for all methane sources and for wetlands. The figure also includes difference maps between the JULES-GIEMS emission estimates and the inverse emission

inventory estimates derived by Bousquet et al. (2011) using emission priors based on the Fung (panels b and e) and Kaplan (panels c and f) wetland data sets. There is some agreement, which is not surprising as similar data sets were used, but that there are also differences, most noticeably in the wetlands. The JULES-GIEMS inventory has some similarities with the inverse inventory using the Kaplan wetland data set (see material and figures in Sect. 1.3 of the Supplement). The monthly GIEMS data set of Prigent et al. (2012) has been used in this work as it provides a long-term global data set derived using a consistent methodology. As part of the wetland model intercomparison, Melton et al. (2013) noted that there were significant differences between this data set and the wetland maps derived by Kaplan (as described in Bergamaschi et al., 2007). The inundation product showed more wetlands in Europe and the Canadian Arctic but fewer in the Hudson Bay Lowlands. Melton et al. (2013) identified a number of reasons for these differences: (i) classification of water bodies and wetlands; (ii) distinguishing agricultural (i.e. man-made) and natural wetlands; (iii) the ability of the inundation product to resolve saturated areas with high water tables close to the surface. Many of these differences can be seen in the difference maps.

4 Conclusions

In this paper, we have evaluated wetland emission estimates derived using the UK community land surface model (JULES) against atmospheric observations of methane, including, for the first time, total methane columns derived from the SCIAMACHY instrument on board the ENVISAT satellite. The modelled atmospheric methane columns were biased low (by 50 ppb) compared to those derived from the SCIAMACHY instrument, a consequence of the faster fall-off in the modelled methane concentrations with altitude than that observed. Constraining the modelled concentrations above 300 hPa with vertically resolved methane data from the HALOE-ACE assimilated TOMCAT output resulted in a significantly better agreement with the SCIAMACHY observations. The model performed significantly better against measurements of surface atmospheric methane concentrations.

The wetland emission totals used in this work were consistent with other recently published estimates, although considerable differences remain between wetlands models, as highlighted in the recent WETCHIMP model intercomparison study (Melton et al., 2013). While progress has been made, the JULES methane emission parameterization overestimates the methane emissions in the tropics and underestimates them at mid-NH and higher-NH latitudes. The use of the GIEMS product to constrain JULES-derived wetland fraction improved the representation of the wetland emissions in JULES and gave a good description of the seasonality observed at surface sites influenced by wetlands, especially at high latitudes. We found that the annual cycles ob-

served in the SCIAMACHY measurements and at many of the surface sites influenced by non-wetland sources could not be reproduced in these HadGEM2 runs. This suggests that the emissions over certain regions (e.g. India and China) are possibly too high and/or the monthly emission patterns for specific sectors are incorrect.

The comparisons presented in this paper have identified areas for improvements in aspects of two components in the HadGEM family of models – the land surface and atmospheric chemistry modules. Current and future work will look to improve (a) the description of wetlands and the associated emissions of methane in JULES through the inclusion of an organic soil type related more closely to peatlands, and (b) understanding and addressing the cause(s) of the faster fall-off, with potentially a particular emphasis on the model's stratospheric transport timescale. The inclusion of whole-domain methane chemistry in UKCA by implementing a combined troposphere–stratosphere chemistry scheme (Telford et al., 2014) may help in this regard. The EO data sets used here (and to be extended in the future) are essential for the future evaluations of JULES, UKCA and the HadGEM family of models.

The Supplement related to this article is available online at doi:10.5194/acp-14-13257-2014-supplement.

References

Beck, V., Gerbig, C., Koch, T., Bela, M. M., Longo, K. M., Freitas, S. R., Kaplan, J. O., Prigent, C., Bergamaschi, P. and Heimann, M.: WRF-Chem simulations in the Amazon region during wet and dry season transitions: evaluation of methane models and wetland inundation maps, Atmos. Chem. Phys., 13, 7961–7982, doi:10.5194/acp-13-7961-2013, 2013.

Beer, R.: TES on the aura mission: scientific objectives, measurements, and analysis overview, IEEE T. Geosci. Remote, 44, 1102–1105, doi:10.1109/TGRS.2005.863716, 2006.

Bergamaschi, P., Frankenberg, C., Meirink, J. F., Krol, M., Dentener, F., Wagner, T., Platt, U., Kaplan, J. O., Körner, S., Heimann, M., Dlugokencky, E. J., and Goede, A.: Satellite chartography of atmospheric methane from SCIAMACHY on board ENVISAT: 2. Evaluation based on inverse model simulations, J. Geophys. Res.-Atmos., 112, D02304, doi:10.1029/2006JD007268, 2007.

Bergamaschi, P., Houweling, S., Segers, A., Krol, M., Frankenberg, C., Scheepmaker, R. A., Dlugokencky, E., Wofsy, S. C., Kort, E. A., Sweeney, C., Schuck, T., Brenninkmeijer, C., Chen, H., Beck, V., and Gerbig, C.: Atmospheric CH_4 in the first decade of the 21st century: inverse modeling analysis using SCIAMACHY satellite retrievals and NOAA surface measurements, J. Geophys. Res.-Atmos., 118, 7350–7369, doi:10.1002/jgrd.50480, 2013.

Bernath, P. F., McElroy, C. T., Abrams, M. C., Boone, C. D., Butler, M., Camy-Peyret, C., Carleer, M., Clerbaux, C., Coheur, P.-F., Colin, R., DeCola, P., DeMazière, M., Drummond, J. R., Dufour, D., Evans, W. F. J., Fast, H., Fussen, D., Gilbert, K., Jennings, D. E., Llewellyn, E. J., Lowe, R. P., Mahieu, E., McConnell, J. C., McHugh, M., McLeod, S. D., Michaud, R., Midwinter, C., Nassar, R., Nichitiu, F., Nowlan, C., Rinsland, C. P., Rochon, Y. J., Rowlands, N., Semeniuk, K., Simon, P., Skelton, R., Sloan, J. J., Soucy, M.-A., Strong, K., Tremblay, P., Turnbull, D., Walker, K. A., Walkty, I., Wardle, D. A., Wehrle, V., Zander, R., and Zou, J.: Atmospheric Chemistry Experiment (ACE): mission overview, Geophys. Res. Lett., 32, L15S01, doi:10.1029/2005GL022386, 2005.

Best, M. J., Pryor, M., Clark, D. B., Rooney, G. G., Essery, R. L. H., Ménard, C. B., Edwards, J. M., Hendry, M. A., Porson, A., Gedney, N., Mercado, L. M., Sitch, S., Blyth, E., Boucher, O., Cox, P. M., Grimmond, C. S. B., and Harding, R. J.: The Joint UK Land Environment Simulator (JULES), model description – Part 1: Energy and water fluxes, Geosci. Model Dev., 4, 677–699, doi:10.5194/gmd-4-677-2011, 2011.

Blake, D. R. and Rowland, F. S.: Continuing worldwide increase in tropospheric methane, 1978 to 1987, Science, 239, 1129–1131, doi:10.1126/science.239.4844.1129, 1988.

Bloom, A. A., Palmer, P. I., Fraser, A., Reay, D. S., and Frankenberg, C.: Large-scale controls of methanogenesis inferred from methane and gravity spaceborne data, Science, 327, 322–325, doi:10.1126/science.1175176, 2010.

Bloom, A. A., Palmer, P. I., Fraser, A., and Reay, D. S.: Seasonal variability of tropical wetland CH_4 emissions: the role of the methanogen-available carbon pool, Biogeosciences, 9, 2821–2830, doi:10.5194/bg-9-2821-2012, 2012.

Blunden, J. and Arndt, D. S.: State of the Climate in 2012, B. Am. Meteorol. Soc., 94, S1–S258, doi:10.1175/2013BAMSStateoftheClimate.1, 2013.

Bousquet, P., Ciais, P., Miller, J. B., Dlugokencky, E. J., Hauglus- taine, D. A., Prigent, C., Van der Werf, G. R., Peylin, P., Brunke, E.-G., Carouge, C., Langenfelds, R. L., Lathiere, J., Papa, F., Ramonet, M., Schmidt, M., Steele, L. P., Tyler, S. C., and White, J.: Contribution of anthropogenic and natural sources to atmospheric methane variability, Nature, 443, 439–443, doi:10.1038/nature05132, 2006.

Bousquet, P., Ringeval, B., Pison, I., Dlugokencky, E. J., Brunke, E.- G., Carouge, C., Chevallier, F., Fortems-Cheiney, A., Franken- berg, C., Hauglustaine, D. A., Krummel, P. B., Langen- felds, R. L., Ramonet, M., Schmidt, M., Steele, L. P., Szopa, S., Yver, C., Viovy, N., and Ciais, P.: Source attribution of the changes in atmospheric methane for 2006–2008, Atmos. Chem. Phys., 11, 3689–3700, doi:10.5194/acp-11-3689-2011, 2011.

Bowerman, N. H. A., Frame, D. J., Huntingford, C., Lowe, J. A., Smith, S. M., and Allen, M. R.: The role of short-lived climate pollutants in meeting temperature goals, Nature Climate Change, 3, 1021–1024, doi:10.1038/nclimate2034, 2013.

Breider, T. J., Chipperfield, M. P., Richards, N. A. D., Carslaw, K. S., Mann, G. W., and Spracklen, D. V.: Impact of BrO on dimethylsulfide in the remote marine boundary layer, Geophys. Res. Lett., 37, L02807, doi:10.1029/2009GL040868, 2010.

Buchwitz, M., de Beek, R., Burrows, J. P., Bovensmann, H., Warneke, T., Notholt, J., Meirink, J. F., Goede, A. P. H., Bergama- schi, P., Körner, S., Heimann, M., and Schulz, A.: Atmospheric methane and carbon dioxide from SCIAMACHY satellite data: initial comparison with chemistry and transport models, Atmos. Chem. Phys., 5, 941–962, doi:10.5194/acp-5-941-2005, 2005.

Buchwitz, M., Reuter, M., Schneising, O., Boesch, H., Guer- let, S., Dils, B., Aben, I., Armante, R., Bergamaschi, P., Blu- menstock, T., Bovensmann, H., Brunner, D., Buchmann, B., Bur- rows, J., Butz, A., Chédin, A., Chevallier, F., Crevoisier, C., Deutscher, N., Frankenberg, C., Hase, F., Hasekamp, O., Hey- mann, J., Kaminski, T., Laeng, A., Lichtenberg, G., Maz- ière, M. D., Noël, S., Notholt, J., Orphal, J., Popp, C., Parker, R., Scholze, M., Sussmann, R., Stiller, G., Warneke, T., Zehner, C., Bril, A., Crisp, D., Griffith, D., Kuze, A., O'Dell, C., Os- hchepkov, S., Sherlock, V., Suto, H., Wennberg, P., Wunch, D., Yokota, T., and Yoshida, Y.: The Greenhouse Gas Climate Change Initiative (GHG-CCI): comparison and quality as- sessment of near-surface-sensitive satellite-derived CO_2 and CH_4 global data sets, Remote Sens. Environ., in press, doi:10.1016/j.rse.2013.04.024, 2013.

Chipperfield, M. P.: New version of the TOMCAT/SLIMCAT off- line chemical transport model: Intercomparison of stratospheric tracer experiments, Q. J. Roy. Meteor. Soc., 132, 1179–1203, doi:10.1256/qj.05.51, 2006.

Chipperfield, M. P., Khattatov, B. V., and Lary, D. J.: Sequential assimilation of stratospheric chemical observations in a three- dimensional model, J. Geophys. Res.-Atmos., 107, ACH 8–1– ACH 8–14, doi:10.1029/2002JD002110, 2002.

Clark, D. B., Mercado, L. M., Sitch, S., Jones, C. D., Gedney, N., Best, M. J., Pryor, M., Rooney, G. G., Essery, R. L. H., Blyth, E., Boucher, O., Harding, R. J., Huntingford, C., and Cox, P. M.: The Joint UK Land Environment Simulator (JULES), model descrip- tion – Part 2: Carbon fluxes and vegetation dynamics, Geosci. Model Dev., 4, 701–722, doi:10.5194/gmd-4-701-2011, 2011.

Collins, W. J., Bellouin, N., Doutriaux-Boucher, M., Gedney, N., Halloran, P., Hinton, T., Hughes, J., Jones, C. D., Joshi, M., Liddicoat, S., Martin, G., O'Connor, F., Rae, J., Senior, C., Sitch, S., Totterdell, I., Wiltshire, A., and Woodward, S.: Devel- opment and evaluation of an Earth-System model – HadGEM2, Geosci. Model Dev., 4, 1051–1075, doi:10.5194/gmd-4-1051- 2011, 2011.

De Mazière, M., Vigouroux, C., Bernath, P. F., Baron, P., Blu- menstock, T., Boone, C., Brogniez, C., Catoire, V., Coffey, M., Duchatelet, P., Griffith, D., Hannigan, J., Kasai, Y., Kramer, I., Jones, N., Mahieu, E., Manney, G. L., Piccolo, C., Randall, C., Robert, C., Senten, C., Strong, K., Taylor, J., Tétard, C., Walker, K. A., and Wood, S.: Validation of ACE-FTS v2.2 methane profiles from the upper troposphere to the lower meso- sphere, Atmos. Chem. Phys., 8, 2421–2435, doi:10.5194/acp-8- 2421-2008, 2008.

Denman, K., Brasseur, G., Chidthaisong, A., Ciais, P., Cox, P., Dickinson, R., Hauglustaine, D., Heinze, C., Holland, E., Ja- cob, D., Lohmann, U., Ramachandran, S., da Silva Dias, P., Wofsy, S., and Zhang, X.: Couplings between changes in the climate system and biogeochemistry, in: Climate Change 2007: The Physical Science Basis, Contribution of Working Group I to the Fourth Assessment Report of the Intergovernmental Panel on Climate Change, edited by: Solomon, S., Qin, D., Man- ning, M., Chen, Z., Marquis, M., Averyt, K. B., Tignor, M., and Miller, H. L., Cambridge University Press, Cambridge, UK and New York, NY, USA, 2007.

Dennis, R., Fox, T., Fuentes, M., Gilliland, A., Hanna, S., Hogrefe, C., Irwin, J., Rao, S., Scheffe, R., Schere, K., Steyn, D., and Venkatram, A.: A framework for evaluating regional–scale numerical photochemical modeling systems, Environ. Fluid Mech., 10, 471–489, doi:10.1007/s10652-009-9163-2, 2010.

Dils, B., Buchwitz, M., Reuter, M., Schneising, O., Boesch, H., Parker, R., Guerlet, S., Aben, I., Blumenstock, T., Bur- rows, J. P., Butz, A., Deutscher, N. M., Frankenberg, C., Hase, F., Hasekamp, O. P., Heymann, J., De Mazière, M., Notholt, J., Suss- mann, R., Warneke, T., Griffith, D., Sherlock, V., Wunch, D.: The Greenhouse Gas Climate Change Initiative (GHG-CCI): com- parative validation of GHG-CCI SCIAMACHY/ENVISAT and TANSO-FTS/GOSAT CO_2 and CH_4 retrieval algorithm prod- ucts with measurements from the TCCON, Atmos. Meas. Tech., 7, 1723–1744, doi:10.5194/amt-7-1723-2014, 2014.

Dlugokencky, E. J., Masaire, K. A., Lang, P. M., Tans, P. P., Steele, L. P., and Nisbet, E. G.: A dramatic decrease in the growth rate of atmospheric methane in the Northern Hemisphere during 1992, Geophys. Res. Lett., 21, 45–48, doi:10.1029/93GL03070, 1994a.

Dlugokencky, E. J., Steele, L. P., Lang, P. M., and Masarie, K. A.: The growth rate and distribution of atmospheric methane, J. Geo- phys. Res.-Atmos., 99, 17021–17043, doi:10.1029/94JD01245, 1994b.

Dlugokencky, E. J., Masarie, K. A., Lang, P. M., and Tans, P. P.: Continuing decline in the growth rate of the atmospheric methane burden, Nature, 393, 447–450, doi:10.1038/30934, 1998.

Dlugokencky, E. J., Walter, B. P., Masarie, K. A., Lang, P. M., and Kasischke, E. S.: Measurements of an anomalous global methane increase during 1998, Geophys. Res. Lett., 28, 499–502, doi:10.1029/2000GL012119, 2001.

Dlugokencky, E. J., Houweling, S., Bruhwiler, L., Masarie, K. A., Lang, P. M., Miller, J. B., and Tans, P. P.: Atmospheric methane levels off: temporary pause or a new steady-state?, Geophys. Res. Lett., 30, 1992, doi:10.1029/2003GL018126, 2003.

Dlugokencky, E. J., Bruhwiler, L., White, J. W. C., Emmons, L. K., Novelli, P. C., Montzka, S. A., Masarie, K. A., Lang, P. M., Crotwell, A. M., Miller, J. B., and Gatti, L. V.: Observational constraints on recent increases in the atmospheric CH$_4$ burden, Geophys. Res. Lett., 36, L18803, doi:10.1029/2009GL039780, 2009.

Dlugokencky, E. J., Nisbet, E. G., Fisher, R., and Lowry, D.: Global atmospheric methane: budget, changes and dangers, Philos. T. R. Soc. A, 369, 2058–2072, doi:10.1098/rsta.2010.0341, 2011.

Dlugokencky, E. J., Lang, P. M., Crotwell, A. M., and Masarie, K. A.: Atmospheric Methane Dry Air Mole Fractions from the NOAA ESRL Carbon Cycle Co-operative Global Air Sampling Network, 1983–2011, Version: 24 September 2012, ftp://aftp.cmdl.noaa.gov/data/trace_gases/ch4/flask/surface/ (last access date of updated and extended dataset: 9 May 2014), 2012.

Forster, P., Ramaswamy, V., Artaxo, P., Berntsen, T., Betts, R., Fahey, D., Haywood, J., Lean, J., Lowe, D., Myhre, G., Nganga, J., Prinn, R., Raga, G., Schulz, M., and Van Dorland, R.: Changes in atmospheric constituents and in radiative forcing, in: Climate Change 2007: The Physical Science Basis, Contribution of Working Group I to the Fourth Assessment Report of the Intergovernmental Panel on Climate Change, edited by: Solomon, S., Qin, D., Manning, M., Chen, Z., Marquis, M., Averyt, K. B., Tignor, M., and Miller, H. L., Cambridge University Press, Cambridge, UK and New York, NY, USA, 2007.

Frankenberg, C., Meirink, J. F., van Weele, M., Platt, U., and Wagner, T.: Assessing methane emissions from global space-borne observations, Science, 308, 1010–1014, doi:10.1126/science.1106644, 2005.

Frankenberg, C., Meirink, J. F., Bergamaschi, P., Goede, A. P. H., Heimann, M., Körner, S., Platt, U., van Weele, M., and Wagner, T.: Satellite chartography of atmospheric methane from SCIAMACHY on board ENVISAT: analysis of the years 2003 and 2004, J. Geophys. Res.-Atmos., 111, D07303, doi:10.1029/2005JD006235, 2006.

Frankenberg, C., Bergamaschi, P., Butz, A., Houweling, S., Meirink, J. F., Notholt, J., Petersen, A. K., Schrijver, H., Warneke, T., and Aben, I.: Tropical methane emissions: a revised view from SCIAMACHY onboard ENVISAT, Geophys. Res. Lett., 35, L15811, doi:10.1029/2008GL034300, 2008.

Fraser, A., Palmer, P. I., Feng, L., Boesch, H., Cogan, A., Parker, R., Dlugokencky, E. J., Fraser, P. J., Krummel, P. B., Langenfelds, R. L., O'Doherty, S., Prinn, R. G., Steele, L. P., van der Schoot, M., and Weiss, R. F.: Estimating regional methane surface fluxes: the relative importance of surface and GOSAT mole fraction measurements, Atmos. Chem. Phys., 13, 5697–5713, doi:10.5194/acp-13-5697-2013, 2013.

Fung, I., John, J., Lerner, J., Matthews, E., Prather, M., Steele, L. P., and Fraser, P. J.: Three-dimensional model synthesis of the global methane cycle, J. Geophys. Res.-Atmos., 96, 13033–13065, doi:10.1029/91JD01247, 1991.

Gedney, N. and Cox, P. M.: The sensitivity of global climate model simulations to the representation of soil moisture heterogeneity, J. Hydrometeorol., 4, 1265–1275, doi:10.1175/1525-7541(2003)004<1265:TSOGCM>2.0.CO;2, 2003.

Gedney, N., Cox, P. M., and Huntingford, C.: Climate feedback from wetland methane emissions, Geophys. Res. Lett., 31, L20503, doi:10.1029/2004GL020919, 2004.

Glagolev, M., Kleptsova, I., Filippov, I., Maksyutov, S., and Machida, T.: Regional methane emission from West Siberia mire landscapes, Environ. Res. Lett., 6, 045214, doi:10.1088/1748-9326/6/4/045214, 2011.

Kim, H.-S., Maksyutov, S., Glagolev, M. V., Machida, T., Patra, P. K., Sudo, K., and Inoue, G.: Evaluation of methane emissions from West Siberian wetlands based on inverse modeling, Environ. Res. Lett., 6, 035201, doi:10.1088/1748-9326/6/3/035201, 2011.

Kirschke, S., Bousquet, P., Ciais, P., Saunois, M., Canadell, J. G., Dlugokencky, E. J., Bergamaschi, P., Bergmann, D., Blake, D. R., Bruhwiler, L., Cameron-Smith, P., Castaldi, S., Chevallier, F., Feng, L., Fraser, A., Heimann, M., Hodson, E. L., Houweling, S., Josse, B., Fraser, P. J., Krummel, P. B., Lamarque, J.-F., Langenfelds, R. L., Le Quere, C., Naik, V., O'Doherty, S., Palmer, P. I., Pison, I., Plummer, D., Poulter, B., Prinn, R. G., Rigby, M., Ringeval, B., Santini, M., Schmidt, M., Shindell, D. T., Simpson, I. J., Spahni, R., Steele, L. P., Strode, S. A., Sudo, K., Szopa, S., van der Werf, G. R., Voulgarakis, A., van Weele, M., Weiss, R. F., Williams, J. E., and Zeng, G.: Three decades of global methane sources and sinks, Nat. Geosci., 6, 813–823, doi:10.1038/ngeo1955, 2013.

Kuze, A., Suto, H., Nakajima, M., and Hamazaki, T.: Thermal and near infrared sensor for carbon observation Fourier-transform spectrometer on the Greenhouse Gases Observing Satellite for greenhouse gases monitoring, Appl. Optics, 48, 6716–6733, doi:10.1364/AO.48.006716, 2009.

Lamarque, J.-F., Bond, T. C., Eyring, V., Granier, C., Heil, A., Klimont, Z., Lee, D., Liousse, C., Mieville, A., Owen, B., Schultz, M. G., Shindell, D., Smith, S. J., Stehfest, E., Van Aardenne, J., Cooper, O. R., Kainuma, M., Mahowald, N., McConnell, J. R., Naik, V., Riahi, K., and van Vuuren, D. P.: Historical (1850–2000) gridded anthropogenic and biomass burning emissions of reactive gases and aerosols: methodology and application, Atmos. Chem. Phys., 10, 7017–7039, doi:10.5194/acp-10-7017-2010, 2010.

Meirink, J. F., Bergamaschi, P., Frankenberg, C., d'Amelio, M. T. S., Dlugokencky, E. J., Gatti, L. V., Houweling, S., Miller, J. B., Röckmann, T., Villani, M. G., and Krol, M. C.: Four-dimensional variational data assimilation for inverse modeling of atmospheric methane emissions: analysis of SCIAMACHY observations, J. Geophys. Res.-Atmos., 113, D17301, doi:10.1029/2007JD009740, 2008.

Melton, J. R., Wania, R., Hodson, E. L., Poulter, B., Ringeval, B., Spahni, R., Bohn, T., Avis, C. A., Beerling, D. J., Chen, G., Eliseev, A. V., Denisov, S. N., Hopcroft, P. O., Lettenmaier, D. P., Riley, W. J., Singarayer, J. S., Subin, Z. M., Tian, H., Zürcher, S., Brovkin, V., van Bodegom, P. M., Kleinen, T., Yu, Z. C., and Kaplan, J. O.: Present state of global wetland extent and wetland methane modelling: conclusions from a model intercomparison project (WETCHIMP), Biogeosciences, 10, 753–788, doi:10.5194/bg-10-753-2013, 2013.

Monks, S. A., Arnold, S. R., and Chipperfield, M. P.: Evidence for El Niño–Southern Oscillation (ENSO) influence on Arctic CO interannual variability through biomass burning emissions, Geophys. Res. Lett., 39, L14804, doi:10.1029/2012GL052512, 2012.

Monteil, G., Houweling, S., Dlugockenky, E. J., Maenhout, G., Vaughn, B. H., White, J. W. C., and Rockmann, T.: Interpreting methane variations in the past two decades using measurements of CH_4 mixing ratio and isotopic composition, Atmos. Chem. Phys., 11, 9141–9153, doi:10.5194/acp-11-9141-2011, 2011.

Morgenstern, O., Braesicke, P., O'Connor, F. M., Bushell, A. C., Johnson, C. E., Osprey, S. M., Pyle, J. A.: Evaluation of the new UKCA climate-composition model – Part 1: The stratosphere, Geosci. Model Dev., 2, 43–57, doi:10.5194/gmd-2-43-2009, 2009.

O'Connor, F. M., Boucher, O., Gedney, N., Jones, C. D., Folberth, G. A., Coppell, R., Friedlingstein, P., Collins, W. J., Chappellaz, J., Ridley, J., and Johnson, C. E.: Possible role of wetlands, permafrost, and methane hydrates in the methane cycle under future climate change: a review, Rev. Geophys., 48, RG4005, doi:10.1029/2010RG000326, 2010.

O'Connor, F. M., Johnson, C. E., Morgenstern, O., Abraham, N. L., Braesicke, P., Dalvi, M., Folberth, G. A., Sanderson, M. G., Telford, P. J., Voulgarakis, A., Young, P. J., Zeng, G., Collins, W. J., and Pyle, J. A.: Evaluation of the new UKCA climate-composition model – Part 2: The Troposphere, Geosci. Model Dev., 7, 41–91, doi:10.5194/gmd-7-41-2014, 2014.

Papa, F., Prigent, C., Durand, F., and Rossow, W. B.: Wetland dynamics using a suite of satellite observations: a case study of application and evaluation for the Indian Subcontinent, Geophys. Res. Lett., 33, L08401, doi:10.1029/2006GL025767, 2006a.

Papa, F., Prigent, C., Rossow, W. B., Legresy, B., and Remy, F.: Inundated wetland dynamics over boreal regions from remote sensing: the use of Topex–Poseidon dual–frequency radar altimeter observations, Int. J. Remote Sens., 27, 4847–4866, doi:10.1080/01431160600675887, 2006b.

Papa, F., Prigent, C., and Rossow, W. B.: Ob' River flood inundations from satellite observations: a relationship with winter snow parameters and river runoff, J. Geophys. Res.-Atmos., 112, D18103, doi:10.1029/2007JD008451, 2007.

Papa, F., Güntner, A., Frappart, F., Prigent, C., and Rossow, W. B.: Variations of surface water extent and water storage in large river basins: a comparison of different global data sources, Geophys. Res. Lett., 35, L11401, doi:10.1029/2008GL033857, 2008a.

Papa, F., Prigent, C., and Rossow, W.: Monitoring flood and discharge variations in the large Siberian rivers from a multi-satellite technique, Surv. Geophys., 29, 297–317, doi:10.1007/s10712-008-9036-0, 2008b.

Papa, F., Prigent, C., Aires, F., Jimenez, C., Rossow, W. B., and Matthews, E.: Interannual variability of surface water extent at the global scale, 1993–2004, J. Geophys. Res.-Atmos., 115, D12111, doi:10.1029/2009JD012674, 2010.

Park, J. H., Russell, J. M., Gordley, L. L., Drayson, S. R., Benner, D. C., McInerney, J. M., Gunson, M. R., Toon, G. C., Sen, B., Blavier, J.-F., Webster, C. R., Zipf, E. C., Erdman, P., Schmidt, U., and Schiller, C.: Validation of Halogen Occultation Experiment CH_4 measurements from the UARS, J. Geophys. Res.-Atmos., 101, 10183–10203, doi:10.1029/95JD02736, 1996.

Patra, P. K., Takigawa, M., Ishijima, K., Choi, B.-C., Cunnold, D., Dlugokencky, E., Fraser, P., Gomez-Pelaez, A., Goo, T.-Y., Kim, J.-S., Krummel, P., Langenfelds, R., Meinhardt, F., Mukai, H., O'Doherty, S., Prinn, R., Simmonds, P., Steele, P., Tohjima, Y., Tsuboi, K., Uhse, K., Weiss, R., Worthy, D.,

Nakazawa, T.: Growth Rate, Seasonal, Synoptic, Diurnal Variations and Budget of Methane in the Lower Atmosphere, J. Met. Soc. Japan. Ser. II, 87, 635–663, doi:10.2151/jmsj.87.635, 2009.

Patra, P. K., Houweling, S., Krol, M., Bousquet, P., Belikov, D., Bergmann, D., Bian, H., Cameron-Smith, P., Chipperfield, M. P., Corbin, K., Fortems-Cheiney, A., Fraser, A., Gloor, E., Hess, P., Ito, A., Kawa, S. R., Law, R. M., Loh, Z., Maksyutov, S., Meng, L., Palmer, P. I., Prinn, R. G., Rigby, M., Saito, R., and Wilson, C.: TransCom model simulations of CH_4 and related species: linking transport, surface flux and chemical loss with CH_4 variability in the troposphere and lower stratosphere, Atmos. Chem. Phys., 11, 12813–12837, doi:10.5194/acp-11-12813-2011, 2011.

Petrescu, A. M. R., van Beek, L. P. H., van Huissteden, J., Prigent, C., Sachs, T., Corradi, C. A. R., Parmentier, F. J. W., and Dolman, A. J.: Modeling regional to global CH_4 emissions of boreal and arctic wetlands, Global Biogeochem. Cy., 24, GB4009, doi:10.1029/2009GB003610, 2010.

Pickett-Heaps, C. A., Jacob, D. J., Wecht, K. J., Kort, E. A., Wofsy, S. C., Diskin, G. S., Worthy, D. E. J., Kaplan, J. O., Bey, I., and Drevet, J.: Magnitude and seasonality of wetland methane emissions from the Hudson Bay Lowlands (Canada), Atmos. Chem. Phys., 11, 3773–3779, doi:10.5194/acp-11-3773-2011, 2011.

Pison, I., Ringeval, B., Bousquet, P., Prigent, C., and Papa, F.: Stable atmospheric methane in the 2000s: key-role of emissions from natural wetlands, Atmos. Chem. Phys., 13, 11609–11623, doi:10.5194/acp-13-11609-2013, 2013.

Portmann, F. T., Siebert, S., and Döll, P.: MIRCA2000 – global monthly irrigated and rainfed crop areas around the year 2000: a new high-resolution data set for agricultural and hydrological modeling, Global Biogeochem. Cy., 24, GB1011, doi:10.1029/2008GB003435, 2010.

Prather, M., Ehhalt, D., Dentener, F., Derwent, R., Dlugokencky, E., Holland, E., Isaksen, I., Katima, J., Kirchhoff, V., Matson, P., Midgley, P., and Wang, M.: Atmospheric Chemistry and Greenhouse Gases, in: Climate Change 2001: The Scientific Basis. Contribution of Working Group I to the Third Assessment Report of the Intergovernmental Panel on Climate Change, edited by: Houghton, J. T., Ding, Y., Griggs, D. J., Noguer, M., van der Linden, P. J., Dai, X., Maskell, K., and Johnson, C. A., Cambridge University Press, Cambridge, United Kingdom and New York, NY, USA, 881 pp., 2001.

Prather, M. J., Holmes, C. D. and Hsu, J.: Reactive greenhouse gas scenarios: Systematic exploration of uncertainties and the role of atmospheric chemistry, Geophys. Res. Lett., 39, L09803, doi:10.1029/2012GL051440, 2012.

Prigent, C., Aires, F., Rossow, W., and Matthews, E.: Joint characterization of vegetation by satellite observations from visible to microwave wavelengths: a sensitivity analysis, J. Geophys. Res.-Atmos., 106, 20665–20685, doi:10.1029/2000JD900801, 2001a.

Prigent, C., Matthews, E., Aires, F., and Rossow, W. B.: Remote sensing of global wetland dynamics with multiple satellite data sets, Geophys. Res. Lett., 28, 4631–4634, doi:10.1029/2001GL013263, 2001b.

Prigent, C., Papa, F., Aires, F., Rossow, W. B., and Matthews, E.: Global inundation dynamics inferred from multiple satellite observations, 1993–2000, J. Geophys. Res.-Atmos., 112, D12107, doi:10.1029/2006JD007847, 2007.

Prigent, C., Papa, F., Aires, F., Jimenez, C., Rossow, W. B., and Matthews, E.: Changes in land surface water dynamics since the 1990s and relation to population pressure, Geophys. Res. Lett., 39, L08403, doi:10.1029/2012GL051276, 2012.

Ramaswamy, V., Boucher, O., Haigh, J., Hauglustaine, D., Haywood, J., Myhre, G., Nakajima, T., Shi, G., and Solomon, S.: 2001: radiative forcing of climate change, in: Climate Change 2001: the Scientific Basis. Contribution of Working Group I to the Third Assessment Report of the Intergovernmental Panel on Climate Change, edited by: Houghton, J. T., Ding, Y., Griggs, D. J., Noguer, M., van der Linden, P. J., Dai, X., Maskell, K., and Johnson, C. A., Cambridge University Press, Cambridge, UK and New York, NY, USA, 349–416, 2001.

Rigby, M., Prinn, R. G., Fraser, P. J., Simmonds, P. G., Langenfelds, R. L., Huang, J., Cunnold, D. M., Steele, L. P., Krummel, P. B., Weiss, R. F., O'Doherty, S., Salameh, P. K., Wang, H. J., Harth, C. M., Mühle, J., and Porter, L. W.: Renewed growth of atmospheric methane, Geophys. Res. Lett., 35, L22805, doi:10.1029/2008GL036037, 2008.

Ringeval, B., de Noblet-Ducoudré, N., Ciais, P., Bousquet, P., Prigent, C., Papa, F., and Rossow, W. B.: An attempt to quantify the impact of changes in wetland extent on methane emissions on the seasonal and interannual time scales, Global Biogeochem. Cy., 24, GB2003, doi:10.1029/2008GB003354, 2010.

Russell, J. M., Gordley, L. L., Park, J. H., Drayson, S. R., Hesketh, W. D., Cicerone, R. J., Tuck, A. F., Frederick, J. E., Harries, J. E., and Crutzen, P. J.: The Halogen Occultation Experiment, J. Geophys. Res.-Atmos., 98, 10777–10797, doi:10.1029/93JD00799, 1993.

Schneising, O., Buchwitz, M., Burrows, J. P., Bovensmann, H., Bergamaschi, P., and Peters, W.: Three years of greenhouse gas column-averaged dry air mole fractions retrieved from satellite – Part 2: Methane, Atmos. Chem. Phys., 9, 443–465, doi:10.5194/acp-9-443-2009, 2009.

Schneising, O., Buchwitz, M., Reuter, M., Heymann, J., Bovensmann, H., and Burrows, J. P.: Long-term analysis of carbon dioxide and methane column-averaged mole fractions retrieved from SCIAMACHY, Atmos. Chem. Phys., 11, 2863–2880, doi:10.5194/acp-11-2863-2011, 2011.

Schneising, O., Bergamaschi, P., Bovensmann, H., Buchwitz, M., Burrows, J. P., Deutscher, N. M., Griffith, D. W. T., Heymann, J., Macatangay, R., Messerschmidt, J., Notholt, J., Rettinger, M., Reuter, M., Sussmann, R., Velazco, V. A., Warneke, T., Wennberg, P. O., and Wunch, D.: Atmospheric greenhouse gases retrieved from SCIAMACHY: comparison to ground-based FTS measurements and model results, Atmos. Chem. Phys., 12, 1527–1540, doi:10.5194/acp-12-1527-2012, 2012.

Shindell, D. T., Faluvegi, G., Koch, D. M., Schmidt, G. A., Unger, N., and Bauer, S. E.: Improved Attribution of Climate Forcing to Emissions, Science, 326, 716–718, doi:10.1126/science.1174760, 2009.

Shindell, D., Kuylenstierna, J. C. I., Vignati, E., van Dingenen, R., Amann, M., Klimont, Z., Anenberg, S. C., Muller, N., Janssens-Maenhout, G., Raes, F., Schwartz, J., Faluvegi, G., Pozzoli, L., Kupiainen, K., Höglund-Isaksson, L., Emberson, L., Streets, D., Ramanathan, V., Hicks, K., Oanh, N. T. K., Milly, G., Williams, M., Demkine, V., and Fowler, D.: Simultaneously mitigating near-term climate change and improving human health and food security, Science, 335, 183–189, doi:10.1126/science.1210026, 2012.

Simmonds, P., Manning, A., Derwent, R., Ciais, P., Ramonet, M., Kazan, V., and Ryall, D.: A burning question. Can recent growth rate anomalies in the greenhouse gases be attributed to large-scale biomass burning events?, Atmos. Environ., 39, 2513–2517, doi:10.1016/j.atmosenv.2005.02.018, 2005.

Steele, L., Fraser, P., Rasmussen, R., Khalil, M., Conway, T., Crawford, A., Gammon, R., Masarie, K., and Thoning, K.: The global distribution of methane in the troposphere, J. Atmos. Chem., 5, 125–171, doi:10.1007/BF00048857, 1987.

Steele, L. P., Dlugokencky, E. J., Lang, P. M., Tans, P. P., Martin, R. C., and Masarie, K. A.: Slowing down of the global accumulation of atmospheric methane during the 1980s, Nature, 358, 313–316, doi:10.1038/358313a0, 1992.

Stevenson, D. S., Dentener, F. J., Schultz, M. G., Ellingsen, K., van Noije, T. P. C., Wild, O., Zeng, G., Amann, M., Atherton, C. S., Bell, N., Bergmann, D. J., Bey, I., Butler, T., Cofala, J., Collins, W. J., Derwent, R. G., Doherty, R. M., Drevet, J., Eskes, H. J., Fiore, A. M., Gauss, M., Hauglustaine, D. A., Horowitz, L. W., Isaksen, I. S. A., Krol, M. C., Lamarque, J.-F., Lawrence, M. G., Montanaro, V., Müller, J.-F., Pitari, G., Prather, M. J., Pyle, J. A., Rast, S., Rodriguez, J. M., Sanderson, M. G., Savage, N. H., Shindell, D. T., Strahan, S. E., Sudo, K., and Szopa, S.: Multimodel ensemble simulations of present-day and near-future tropospheric ozone, J. Geophys. Res.-Atmos., 111, D08301, doi:10.1029/2005JD006338, 2006.

Taylor, K. E.: Summarizing multiple aspects of model performance in a single diagram, J. Geophys. Res.-Atmos., 106, 7183–7192, doi:10.1029/2000JD900719, 2001.

Telford, P. J., Archibald, A. T., Abraham, N. L., Braesicke, P., Dalvi, M., Hommel, R., Keeble, J. M., Johnson, C. E, O'Connor, F. M., Squire, O. J., and Pyle, J. A.: Evaluation of the UM-UKCA model configuration for Chemistry of the Stratosphere and Troposphere (CheST), Geosci. Model Dev., in preparation, 2014.

Telford, P. J., Braesicke, P., Morgenstern, O., and Pyle, J. A.: Technical Note: Description and assessment of a nudged version of the new dynamics Unified Model, Atmos. Chem. Phys., 8, 1701–1712, doi:10.5194/acp-8-1701-2008, 2008.

Uppala, S. M., Kållberg, P. W., Simmons, A. J., Andrae, U., Bechtold, V. D. C., Fiorino, M., Gibson, J. K., Haseler, J., Hernandez, A., Kelly, G. A., Li, X., Onogi, K., Saarinen, S., Sokka, N., Allan, R. P., Andersson, E., Arpe, K., Balmaseda, M. A., Beljaars, A. C. M., Berg, L. V. D., Bidlot, J., Bormann, N., Caires, S., Chevallier, F., Dethof, A., Dragosavac, M., Fisher, M., Fuentes, M., Hagemann, S., Hólm, E., Hoskins, B. J., Isaksen, L., Janssen, P. A. E. M., Jenne, R., Mcnally, A. P., Mahfouf, J.-F., Morcrette, J.-J., Rayner, N. A., Saunders, R. W., Simon, P., Sterl, A., Trenberth, K. E., Untch, A., Vasiljevic, D., Viterbo, P., and Woollen, J.: The ERA-40 re-analysis, Q. J. Roy. Meteor. Soc., 131, 2961–3012, doi:10.1256/qj.04.176, 2005.

USEPA: Methane and nitrous oxide emissions from natural sources, Report (EPA 430-R-10-001) of the United States Environmental Protection Agency (Office of Atmospheric Programs), available at: http://www.epa.gov/methane/pdfs/Methane-and-Nitrous-Oxide-Emissions-From-Natural-Sources.pdf (last access: 9 May 2014), 2010.

van der Werf, G. R., Randerson, J. T., Giglio, L., Collatz, G. J., Mu, M., Kasibhatla, P. S., Morton, D. C., DeFries, R. S.,

Jin, Y., and van Leeuwen, T. T.: Global fire emissions and the contribution of deforestation, savanna, forest, agricultural, and peat fires (1997–2009), Atmos. Chem. Phys., 10, 11707–11735, doi:10.5194/acp-10-11707-2010, 2010.

Viovy, N. and Ciais, P.: A combined dataset for ecosystem modelling, available at: http://dods.extra.cea.fr/store/p529viov/cruncep/V4_1901_2012/ (last access date of updated and extended dataset: 9 May 2014), 2009.

Worden, J., Kulawik, S., Frankenberg, C., Payne, V., Bowman, K., Cady-Peirara, K., Wecht, K., Lee, J.-E., and Noone, D.: Profiles of CH_4, HDO, H_2O, and N_2O with improved lower tropospheric vertical resolution from Aura TES radiances, Atmos. Meas. Tech., 5, 397–411, doi:10.5194/amt-5-397-2012, 2012.

Yu, S., Eder, B., Dennis, R., Chu, S.-H., and Schwartz, S. E.: New unbiased symmetric metrics for evaluation of air quality models, Atmos. Sci. Lett., 7, 26–34, doi:10.1002/asl.125, 2006.

Zahn, A., Franz, P., Bechtel, C., Grooß, J.-U., and Röckmann, T.: Modelling the budget of middle atmospheric water vapour isotopes, Atmos. Chem. Phys., 6, 2073–2090, doi:10.5194/acp-6-2073-2006, 2006.